Fascin inhibitor increases intratumoral dendritic cell activation and anti-cancer immunity

Yufeng Wang[1], **Mei Song**[2], **Ming Liu**[3], **Guoan Zhang**[4], **Xian Zhang**[3], **Ming O. Li**[3], **Xiaojing Ma**[2,6], **J. Jillian Zhang**[5], **Xin-Yun Huang**[1,6,7,*]

[1]Department of Physiology and Biophysics, Weill Cornell Medical College of Cornell University, New York, NY 10065, USA

[2]Department of Microbiology and Immunology, Weill Cornell Medical College of Cornell University, New York, NY 10065, USA

[4]Proteomics and Metabolomics Core Facility, Weill Cornell Medical College of Cornell University, New York, NY 10065, USA

[3]Program in Immunology, Memorial Sloan Kettering Cancer Center, New York, NY 10065, USA

[5]Novita Pharmaceuticals, Inc., New York, NY 10065, USA

[6]Sandra and Edward Meyer Cancer Center, Weill Cornell Medicine of Cornell University, New York, NY 10065, USA

[7]Lead contact

SUMMARY

Fascin protein is the main actin-bundling protein in filopodia and invadopodia, which are critical for tumor cell migration, invasion, and metastasis. Small-molecule fascin inhibitors block tumor invasion and metastasis and increase the overall survival of tumor-bearing mice. Here, we report a finding that fascin blockade additionally reinvigorates anti-tumor immune response in syngeneic mouse models of various cancers. Fascin protein levels are increased in conventional dendritic cells (cDCs) in the tumor microenvironment. Mechanistically, fascin inhibitor NP-G2–044 increases the number of intratumoral-activated cDCs and enhances the antigen uptake by cDCs. Furthermore, together with PD-1 blocking antibody, NP-G2–044 markedly increases the number of activated CD8$^+$ T cells in the otherwise anti-PD-1 refractory tumors. Reduction of fascin levels in cDCs, but not fascin gene knockout in tumor cells, mimics the anti-tumor immune effect of NP-G2–044. These data demonstrate that fascin inhibitor NP-G2–044 simultaneously limits tumor metastasis and reinvigorates anti-tumor immune responses.

*Correspondence: xyhuang@med.cornell.edu.

Graphical Abstract
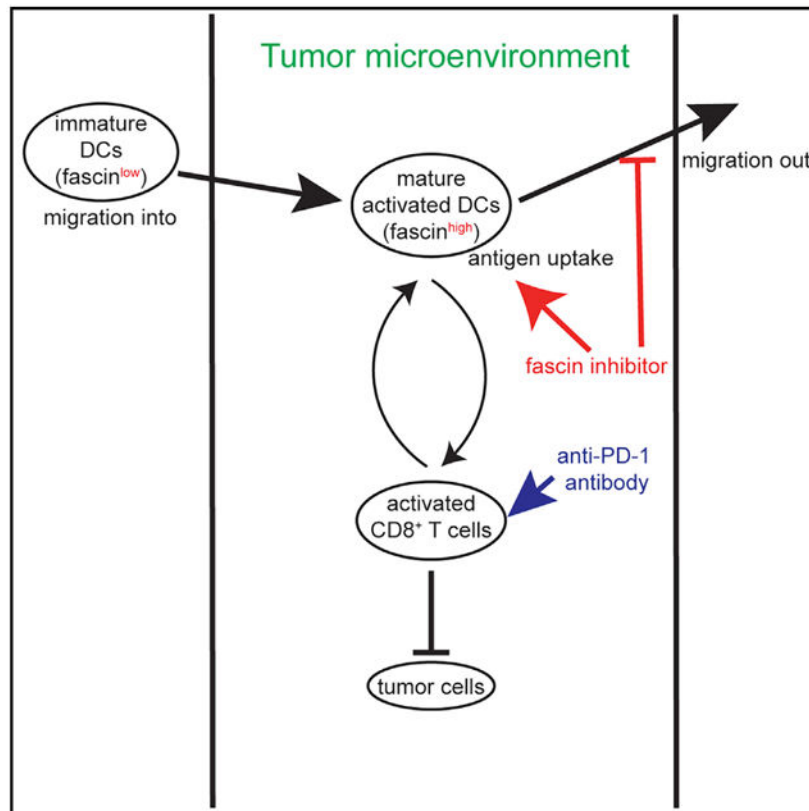
In brief

Wang et al. report that fascin inhibitors act on intratumoral dendritic cells to block the migration and increase the antigen uptake. Together with anti-PD-1 antibody, fascin inhibitors increase the number of intratumoral proliferating and activated CD8$^+$ T cells and the overall survival of mice bearing the otherwise anti-PD-1 refractory tumors.

INTRODUCTION

Fascin is the main actin cross-linker in filopodia and shows no amino acid sequence homology with other actin-binding proteins (Bryan and Kane, 1978; Hashimoto et al., 2011; Li et al., 2014; Mattila and Lappalainen, 2008; Otto et al., 1979; Schoumacher et al., 2014; Tan et al., 2013; Yamashiro-Matsumura and Matsumura, 1985). Fascin regulates actin cytoskeletal reorganization during filopodial formation, lamellipodial formation, stress fiber formation, and focal adhesion turnover (Elkhatib et al., 2014; Han et al., 2016). Elevated levels of fascin have been found in many types of metastatic tumors and are correlated with clinically aggressive phenotypes, poor prognosis, and shorter survival (Tan et al., 2013). Human fascin expression is low or absent in normal adult epithelial cells but highly expressed in metastatic tumors (Grothey et al., 2000; Hashimoto et al., 2005; Snyder et al., 2011, 2014). Mouse genetic studies have shown that deletion of the fascin gene delayed tumor development, slowed the tumor growth, reduced metastatic colonization, and

increased overall survival in a mouse model of pancreatic cancer (Li et al., 2014). Conversely, transgenic expression of fascin in mouse intestinal epithelium increased the tumor incidence, promoted tumor progression, and decreased the overall survival (Schoumacher et al., 2014). We previously screened chemical libraries and identified small-molecule compounds that specifically inhibit the biochemical function of fascin to bundle actin filaments (Chen et al., 2010; Han et al., 2016; Huang et al., 2015; Wang et al., 2020). X-ray crystal structural studies revealed that the fascin inhibitor occupies one actin-binding site and induces a large conformational change of fascin to impair the actin-bundling function of fascin (Huang et al., 2018; Yang et al., 2013).

Cancer care has changed dramatically since the approval of the immune checkpoint inhibitors (ICIs). Yet, significant unmet medical needs remain. In indications such as melanoma and non-small-cell lung cancer (NSLCL), ICIs are having a major impact on a subset of patients, but they need to be enhanced to expand the treatment-responsive patient population. In other indications such as pancreatic cancer, new drugs (such as pioneering alternative immunomodulatory strategies) to partner with ICIs are needed for the immunotherapy concept to work at all. Cancer immunotherapy uses a patient's own immune system to help fight cancer. Tumor cells suppress immune responses by activating negative regulatory pathways (also called checkpoints) that are associated with immune homeostasis or by adopting features that enable them to escape detection (Sharma and Allison, 2015). Two such checkpoints called CTLA-4 and PD-1 have garnered the most attention. The cell-surface receptor PD-1 is expressed by T cells on activation during priming or expansion and binds to one of the two ligands PD-L1 and PD-L2 (Chen and Mellman, 2017). Blocking these checkpoints elicits anti-tumor responses in mice and in cancer patients. However, up to ~85% of patients present with innate or acquired resistance to ICIs, limiting its clinical utility. Here, we discover that fascin blockade can serve as a cancer immunotherapy. Fascin inhibitor can act on dendritic cells (DCs) within the tumor microenvironment (TME). Given the current low response rates to ICIs in the clinics, fascin inhibitors might provide improvements in the clinical care of cancer patients.

RESULTS

NP-G2–044 increases overall survival synergistically with ICIs

We started by investigating whether anti-metastasis agents, such as fascin inhibitors, could be used in combination therapy with ICIs. We explored the effects on the overall survival of tumor-bearing mice of combining ICIs and a fascin inhibitor, NP-G2–044, which blocks tumor cell migration, invasion, and metastasis (Han et al., 2016; Huang et al., 2015, 2018; Wang et al., 2020). We first used the syngeneic model of the poorly immunogenic 4T1 mouse triple-negative breast tumor cells in BALB/c mice with an intact immune system. 4T1 tumor cells are considered to be refractory to ICI treatments (Charles River Laboratories syngeneic mouse models, https://www.criver.com/resources/syngeneic-model-data). 4T1 tumor cells were originally derived from a spontaneously arising mammary tumor in BALB/c mice that aggressively metastasizes, causing a uniformly lethal disease (Pulaski and Ostrand-Rosenberg, 1998). 4T1 tumor cells were implanted into the mammary gland of BALB/c mice, and tumor-bearing mice were randomized into control or treatment groups

(Figures 1A and 1B). In one cohort, control immunoglobulin G (IgG) was given. In the second group, the mice were treated with NP-G2–044. The third group was given ICIs (a combination of anti-PD-1 antibody and anti-CTLA-4 antibody) on days 11, 13, 15, and 17 (Kim et al., 2014). The fourth group of mice was treated with NP-G2–044 combined with ICIs. In this 4T1 mouse model, metastases to lungs could be detected by day 7 post-tumor implantation (DuPré et al., 2007). Because some cancer patients are with metastatic diseases when presented in the clinics, NP-G2–044 treatment was started on day 7. Compared with the control group, NP-G2–044 treatment increased the median overall survival by ~29% (Figure 1B; Table S1A). The ICIs increased the median overall survival by ~27% (Figure 1B; Table S1A). A combination of NP-G2–044 and ICIs increased the median overall survival by ~105%, which is more than tripled the effect by the ICIs alone or NP-G2–044 alone (Figure 1B; Table S1A). These data demonstrate that NP-G2–044 can synergize with ICIs in orthotopic mouse models of 4T1 breast tumors.

To investigate whether this synergistic effect might be limited to 4T1 tumors, we used EMT6 mouse triple-negative breast tumor cells that are moderately responsive to ICIs (Charles River Laboratories syngeneic mouse models) (Figures 1C and 1D). EMT6 tumor-bearing BALB/c mice were randomized into four groups. NP-G2–044 alone had no effect on EMT6 primary tumor growth, as we previously observed for 4T1 breast tumor cells (Han et al., 2016; Huang et al., 2015; Figure 1C). The ICIs (anti-PD-1 and anti-CTLA-4 antibodies) moderately slowed the EMT6 primary tumor growth (Figure 1C). NP-G2–044 and the ICIs together markedly reduced the EMT6 primary tumor growth (Figure 1C). In these experiments, the primary tumor growth was monitored until all mice died. Compared with the control group, NP-G2–044 treatment increased the median overall survival by 63% (Figure 1D; Table S1B). The ICIs increased the median overall survival by 39% (Figure 1D; Table S1B). A combination of NP-G2–044 and ICIs increased the median overall survival by 115%, again demonstrating a synergic effect between NP-G2–044 and the ICIs.

The above two syngeneic models used BALB/c mice. We next used a different mouse strain to investigate the synergistic effect of NP-G2–044 and ICIs. We used the LLC (Lewis Lung Cancer) and Pan02 pancreatic syngeneic models with C57BL/6 mice. Both of these two tumor cells are characterized as refractory to ICI treatments (Charles River Laboratories syngeneic mouse models). LLC tumor cells were implanted into mouse lungs, and tumor-bearing C57BL/6 mice were randomized into four groups. Compared with the control group, NP-G2–044 treatment increased the median overall survival by 33% (Figure 1E; Table S1C). The ICIs increased the median overall survival by 67% (Figure 1E; Table S1C). A combination of NP-G2–044 and ICIs increased the median overall survival by 133% (Figure 1E; Table S1C). In the syngeneic model of pancreatic cancers, Pan02 tumor cells were implanted into the mouse spleen, and tumor-bearing mice were randomized into four groups. Comparing with the control group, NP-G2–044 treatment increased the median overall survival by 13% (Figure 1F; Table S1D). The ICIs increased the median overall survival by 8% (Figure 1F; Table S1D). A combination of NP-G2–044 and ICIs increased the median overall survival by 83% (Figure 1F; Table S1D). Moreover, we also studied the mouse neuroendocrine prostate cancer PNEC30 cells that are resistant to ICI treatments (Charles River Laboratories syngeneic mouse models). We used the BALB/c syngeneic mouse model, and PNEC30 tumor cells were implanted into the mouse prostate. Tumor-bearing mice were

randomized into four groups. Compared with the control group, NP-G2–044 treatment increased the median overall survival by 10% (Figure 1G; Table S1E). The ICIs increased the median overall survival by 45% (Figure 1G; Table S1E). A combination of NP-G2–044 and ICIs increased the median overall survival by 67% (Figure 1G; Table S1E). Together, the above data strongly demonstrate that a fascin inhibitor and ICIs act synergistically to increase the overall survival of tumor-bearing mice.

In the above experiments, we used both anti-PD-1 antibody and anti-CTLA-4 antibody for the ICI immunotherapy. To determine whether the synergistic therapeutic effect with NP-G2–044 requires both the anti-PD-1 antibody and anti-CTLA-4 antibody, treatments with individual antibodies were performed. 4T1 tumor-bearing BALB/c mice were randomized into eight groups. NP-G2–044 alone, anti-CTLA-4 antibody alone, or anti-CTLA-4 antibody together with NP-G2–044 had no effect on 4T1 primary tumor growth (Figure 2A). Anti-PD-1 alone or anti-PD-1 antibody together with anti-CTLA-4 antibody moderately slowed the 4T1 primary tumor growth (Figure 2A). NP-G2–044 with anti-PD-1 antibody and NP-G2–044 with anti-PD-1 antibody + anti-CTLA-4 antibody markedly reduced the 4T1 primary tumor growth (Figure 2A). In these experiments, fewer 4T1 tumor cells were injected into each mouse than in the experiments presented in Figure 1B, and the primary tumor growth was monitored until all mice died. Compared with the control group, NP-G2–044 treatment increased the median overall survival by 68% (Figure 2B; Table S2A). Anti-CTLA-4 antibody alone increased the median overall survival by 25% (Figure 2B; Table S2A). Anti-PD-1 antibody alone increased the median overall survival by 79% (Figure 2B; Table S2A). Combining anti-CTLA-4 and anti-PD-1 antibodies increased the median overall survival by 79% (Figure 2B; Table S2A). Although combining NP-G2–044 with anti-CTLA-4 antibody did not increase the overall survival compared with NP-G2–044 alone (52% versus 68%), the combination of NP-G2–044 with anti-PD-1 antibody dramatically increased the survival by 234% (Figure 2B; Table S2A). More importantly, treatments with NP-G2–044 + anti-PD-1 antibody or with NP-G2–044 + anti-PD-1 antibody + anti-CTLA-4 antibody increased the overall survival of 4T1 tumor-bearing mice to a similar extent (Figure 2B; Table S2A). With or without anti-CTLA-4 antibody did not statistically affect the beneficial outcomes (Figure 2B; Table S2A). Hence, the synergistic effect is due to the combination of NP-G2–044 and anti-PD-1 antibody. To further confirm the synergistic effect of NP-G2–044 with anti-PD-1 antibody alone, we investigated the effect of the combination therapy of NP-G2–044 + anti-PD-1 antibody (without anti-CTLA-4 antibody) by using liver and kidney cancer syngeneic mouse models (Figures 2C and 2D; Tables S2B and S2C). In both cases, NP-G2–044 and anti-PD-1 antibody functioned synergistically to increase the overall survival of tumor-bearing mice (Figure 2C and 2D; Tables S2B and S2C). These data affirm that anti-PD-1 antibody alone (without anti-CTLA-4 antibody) could synergistically function with NP-G2–044 to increase the overall survival.

NP-G2–044 promotes intratumoral DC accumulation and activation

Because NP-G2–044 itself had no effect on the growth of EMT6 and 4T1 primary tumors (Figures 1C and 2A), the marked decrease of primary tumor growth in mice treated with NP-G2–044 and ICIs suggests there is a stronger immune response within the primary tumor tissues of these tumor-bearing mice. Therefore we investigated the effect of NP-G2–044 on

the immune cells within the primary TME. First, we examined which types of immune cells within the TME expressed the highest levels of fascin proteins and, thus, the likely targeted immune cell types. We dissected the primary tumor tissues from host mice. As a control, we also isolated the spleens from tumor-bearing mice and naive mice. Using fluorescence activated cell sorting (FACS), we examined the fascin protein expression levels in various types of immune cells, including CD8$^+$ T cells, CD4$^+$ T cells, regulatory T cells (Tregs), B cells, natural killer (NK) cells, conventional DC type 1 (cDC1) and cDC2 cells, tumor-associated macrophages (TAMs), and MDSCs (myeloid-derived suppressor cells), as well as cancer-associated fibroblasts (CAFs) and endothelial cells (ECs) within the primary tumors (Figure 3A). Fascin protein levels in the spleens of naive mice and of tumor-bearing mice were low (Figure 3A). Fascin protein expression was markedly induced in cDC1 (by ~17-fold), cDC2 (by ~19-fold), and TAM cells (by ~14-fold) in the primary tumor tissues compared with the levels of the same types of cells in the spleens of the tumor-bearing mice (Figure 3A).

Furthermore, we investigated the broad effect of fascin inhibition on the TME by using immune cell profiling and proteomic mass spectrometry. First, we examined the effect of NP-G2–044 on the immune cell composition within the TME. Tumor tissues from four groups of 4T1 tumor-bearing mice (control, NP-G2–044 treated, anti-PD-1 antibody treated, and treatment with NP-G2–044 + anti-PD-1 antibody) were analyzed by FACS for different types of immune cells. This immune cell profiling revealed that NP-G2–044 treatment increased the numbers of cDC1, cDC2, TAMs, neutrophils, and monocytes within the TME (Figures 3B–3D and S1). The combination treatment with NP-G2–044 + anti-PD-1 antibody additionally increased the numbers of CD8$^+$ T cells, CD4$^+$ T cells, and NK cells (Figure 3D). Furthermore, the increase in the numbers of CD8$^+$ T cells and DCs in the tumor tissues by the combination treatment was confirmed by the immunofluorescence staining of the tumor tissues (Figure 3E). The increases of intratumoral cDCs and CD8$^+$ T cells were also observed in mouse models with LLC lung cancer cells (Figure S1).

We then used proteomic mass spectrometry to analyze the changes of proteins within the TME induced by NP-G2–044. Tumor tissues from four groups of 4T1 tumor-bearing mice (control, NP-G2–044 treated, anti-PD-1 antibody treated, and treatment with NP-G2–044 + anti-PD-1 antibody) were analyzed by liquid chromatography-tandem mass spectrometry (LC-MS/MS) (Figures S2–S4). When the proteomic data from the NP-G2–044-treated group were compared with those of the control group, there were ~180 proteins with significantly ($p < 0.05$) changed amounts (Figure S2). When these proteins with significant changes in amounts were analyzed for their interaction networks, there were two main clusters of proteins (Figure S2). One cluster is related to the increased interferon-γ signaling, including proteins Ifi44, Ifitm3, Ifi204, Isg15, Oas1A, and Psmb10 (Figure S2). Another cluster is associated with the decreased anti-inflammatory response, including protease inhibitors Serpina3m, Serpina3n, and Serpina1d (Figure S2). Given the roles of interferons in inflammation, it appears that NP-G2–044 treatment induces an inflamed TME. When the proteomic data from the group treated with NP-G2–044 + anti-PD-1 were compared with those of the group treated with anti-PD-1 antibody, there were ~350 proteins with significantly ($p < 0.05$) changed amounts (Figure S2). When these proteins with significant changes in amounts were analyzed for their interaction networks, there were four main

clusters of proteins (Figure S3). The proteins with increased amounts included proteins involved in vesicle-mediated transport and clathrin-mediated endocytosis (such as Agfg1, Gak, Eps15, Ap1m1, Ap1b1, and Cltc). The proteins with decreased amounts included protein involved in mitochondrial functions (such as Ndufb4, Ndufa6, Ndufb3, and Mt-Co3), actin cytoskeleton (such as Acta1, Actn3, Myh3, Myh7, Tpm1, and Tpm2), and gene expression (such as Ddx5, Dhx9, Ddx49, and Ppie) (Figure S3). When the proteomic data from group treated the NP-G2–044 + anti-PD-1 antibody were compared with that of the other three groups (control, NP-G2–044 treated, anti-PD-1 antibody treated), the proteins with increased amounts included proteins involved in vesicle-mediated transport (Figure S4). The proteins with decreased amounts included proteins involved in mitochondrial functions (Figure S4). The increase of proteins involved in vesicle-mediated transport might include the enhancement of antigen uptake, processing, and presentation because these immune functions involve intracellular protein trafficking (Mellman and Steinman, 2001). Taken together, the above immune cell profiling and proteomic analyses demonstrate that NP-G2–044 has a broad effect on the TME.

Because PD-1 blockade releases the break on intratumoral $CD8^+$ T cells and the major function of DCs is to present antigens to T cells leading to the activation of T cells, we investigated whether the combination treatment with NP-G2–044 and anti-PD-1 antibody leads to the activation and proliferation of intratumoral DCs and $CD8^+$ cytotoxic T cells. First, we examined the activation of intratumoral DCs by measuring the expression levels of three activation markers (CD40, CD80, and CD86) on the intratumoral DCs (Steinman, 1991). As shown in Figures 4A–4C, the expression levels of CD40, CD80, and CD86 were all increased after treatment with NP-G2–044 + anti-PD-1 antibody compared with the other groups. Furthermore, as shown above, NP-G2–044 increased the number of total DCs in the tumor tissues (Figures 3B–3D). This increase of intratumoral DCs might be due to the blockage of DCs migrating out of the tumor tissues because NP-G2–044 could block the migration of DCs, as shown in a Boyden chamber migration assay (Figure 4D). These data are consistent with the observation that fascin gene knockout mice showed reduced (by ~50%) migration of Langerhans cells (a type of DCs in the skin) into lymph nodes (Yamakita et al., 2011). Next we examined the activation of intratumoral $CD8^+$ T cells. The PD-L1/PD-1 signaling axis inhibits the proliferation of cytotoxic $CD8^+$ T cells (Ott et al., 2017; Sharma and Allison, 2015). Anti-PD-1 antibody blocks this PD-L1/PD-1 interaction, partially restores the cytotoxic function of $CD8^+$ T cells, and leads to the killing of tumor cells (Wei et al., 2018). Effector $CD8^+$ T cells express high levels of cytotoxic molecules such as granzymes and perforin (Barry and Bleackley, 2002). As shown in Figure 4E, the combination therapy of NP-G2–044 + anti-PD-1 antibody increased the number of $CD8^+$ killer T cells in the tumor tissues. Moreover, the numbers of activated (Granzyme B^+), proliferating (Ki67$^+$), and activated proliferating (Granzyme B^+ and Ki67$^+$) $CD8^+$ killer T cells were also increased after treatment of NP-G2–044 + anti-PD-1 antibody compared with the control, NP-G2–044-treated, and anti-PD-1 antibody-treated groups (Figures 4F–4H). Additionally, treatments with fascin inhibitors alone or in combination with anti-PD-1 antibody did not change PD-L1 expression on tumor cells (Figures S5A and S5B). NP-G2–044 treatment did not change the expression levels of PD-1 in $CD8^+$ T cells (Figure S5C). Our data suggest that the increases of intratumoral activated $CD8^+$ killer T cells are likely

underlying the inhibitory effect of the combination therapy of NP-G2–044 + anti-PD-1 antibody on the growth of primary tumors and the increase in the overall survival of tumor-bearing mice that we observed above.

Fascin inhibition in DCs is critical for the anti-tumor immune response

To determine if fascin in DCs or in tumor cells is responsible for the synergistic anti-tumor immune effects, the fascin gene was deleted in tumor cells, or fascin protein levels were downregulated in DCs, and then the effect on overall survival of tumor-bearing mice was examined after the combination therapy with NP-G2–044 + the ICIs. Fascin gene was deleted (by CRISPR) in LLC tumor cells (Lin et al., 2019), and this deletion was confirmed by the absence of fascin protein in the knockout cells (Figure 5A). Fascin deletion abolished the inhibitory effect of NP-G2–044 on LLC cell migration (Figure 5B). *Fascin*$^{-/-}$ LLC tumor cells were implanted into the mouse lungs. The mice were randomly divided into four groups (Figures 5C and S5D). If fascin in LLC tumor cells was responsible for the synergistic effect with ICIs, one would expect that fascin gene deletion in LLC cells would mimic NP-G2–044 treatment, and ICIs alone should produce similar effects as the combination therapy (NP-G2–044 + ICIs). As shown in Figures 5C and S7D, although NP-G2–044 + ICIs markedly increase the overall survival of tumor-bearing mice, ICIs alone did not. These results suggest that fascin in LLC tumor cells is not responsible for the synergistic effect. On the other hand, the following data from the mixed bone marrow chimera experiments demonstrate that fascin in DCs is responsible for the synergistic immune effect. Fascin protein levels in DCs (isolated from mouse bone marrow) were knocked down by stable short hairpin RNAs (shRNAs) against fascin (Figure 5D). Host mice were irradiated and transplanted with control (empty vector infected) or fascin-downregulated DCs mixed with DC-depleted (using anti-CD11c antibody) bone marrow cells. These mice (transplanted with control or fascin-downregulated DCs) were implanted with LLC tumor cells and treated with the control solvent, NP-G2–044, anti-PD-1 antibody, or NP-G2–044 + anti-PD-1 antibody (Figure 5E). If fascin protein in DCs is responsible for the synergistic effect, its downregulation in DCs would mimic NP-G2–044 treatment. This would be reflected by the similar effect of anti-PD-1 antibody alone treatment and the combination therapy of NP-G2–044 + anti-PD-1 antibody. Indeed that was what we observed (Figure 5E). Both anti-PD-1 antibody alone and the combination therapy with NP-G2–044 + anti-PD-1 antibody prolonged the overall survival of tumor-bearing mice to a similar extent, compared with that of mice in the control groups (Figure 5E). Together, these data demonstrate that inhibition of fascin proteins in DCs, but not in tumor cells, is responsible for the synergistic effect with anti-PD-1 antibody.

To confirm the essential role of DCs in the NP-G2–044 effect on the anti-tumor immune response, we used *Batf3*$^{-/-}$ host mice (Figure 5F). Batf3 is a transcription factor that is critical for cDC1 cell development (Hildner et al., 2008). In *Batf3*$^{-/-}$ mice, there are no cDC1 cells (Hildner et al., 2008). We orthotopically administered LLC tumor cells into the lungs of wild-type C57BL/6 mice and *Batf3*$^{-/-}$ mice, and these mice were treated with the combination therapy with NP-G2–044 + ICIs. Although wild-type mice treated with NP-G2–044 + ICIs increased the overall survival compared with mice treated with control antibody, survival of *Batf3*$^{-/-}$ mice treated with NP-G2–044 + ICIs was similar to that of

wild-type mice treated with control antibody (Figure 5F). Altogether, the above data demonstrate that DCs are essential for the synergistic anti-tumor immune response by fascin inhibitors and ICIs.

NP-G2–044 increases the antigen uptake by DCs

To further understand the mechanism of action of NP-G2–044 on DCs (in addition to the above described role in DC migration), we investigated the effect of NP-G2–044 on the antigen uptake by DCs. To quantify the antigen uptake, we used two assays with fluorescently labeled dextran or BSA (Hodakoski et al., 2019; Figures 6A–6C). cDC1 cells were plated in 12-well plates containing glass coverslips (Smita et al., 2018). After attachment, cells were incubated with NP-G2–044 and Cascade Blue-labeled dextran or Alexa-Fluor-488-labeled BSA. Uptake of fluorescently labeled dextran or BSA by DCs was then quantified by calculating the total area of internalized fluorescent dextran or BSA normalized to the total area of cells or nuclei, as described (Commisso et al., 2014; Figures 6A–6C). In both studies, NP-G2–044 increased the antigen uptake by DCs (Figures 6A–6C).

To understand the enhancement of antigen uptake by DCs after NP-G2–044 treatment, we investigated the reorganization of the actin cytoskeleton in DCs because antigen uptake (endocytosis) depends on the actin cytoskeleton and fascin is an actin-bundling protein. The antigen uptake and migration of DCs are antagonistic processes (Chabaud et al., 2015). These two cellular events are linked by the dynamic turnover of podosomes, an F-actin-based cell adhesion structure (Gimona et al., 2008). Podosomes provide the adhesion force and extracellular matrix degradation for DC migration (Gimona et al., 2008). On the other hand, podosomes interfere with antigen uptake (West et al., 2004). Podosomes were analyzed by staining DCs with an antibody against the podosome-associated protein vinculin (Figures 6B and 6D). The percentage of cells with podosome structures was quantified (Figure 6D). NP-G2–044 decreased the percentage of DCs with podosomes, as indicated by the vinculin staining (Figures 6B and 6D). These data are consistent with the above observed effect on the functions of DCs (decreased migration and increased antigen uptake) after NP-G2–044 treatment.

Furthermore, we investigated the effect of NP-G2–044 on the antigen uptake in mice (Figure 6E). 4T1 breast tumor cells stably expressing GFP were injected into the mammary glands of host mice. The mice were then treated with or without NP-G2–044. After 20 days, DCs and macrophages were isolated, and GFP[+] DCs and macrophages were quantified (Figure 6E). The results showed that NP-G2–044 treatment increased the number of GFP[+] DCs, but not GFP[+] macrophages (Figure 6E). Together, the above data demonstrate that NP-G2–044 treatment increases the antigen uptake by DCs *in vitro* and *in vivo*.

Increase of the number of intratumoral TLSs

Our data that NP-G2–044 blocks the migration of DCs and induces the accumulation of activated DCs in the TME and that NP-G2–044 + anti-PD-1 antibody increase the activation of CD8^{+} T cells within the TME suggest that DCs might activate CD8^{+} T cells in the TME, possibly in tumor-associated tertiary lymphoid structures (TLSs) (Cabrita et al., 2020; Helmink et al., 2020; Petitprez et al., 2020; Sharonov et al., 2020). TLSs support the

development of tumor-specific T cell responses (Sautès-Fridman et al., 2019). The presence of TLSs has been found to be a positive prognostic marker for ICI treatments of cancer patients (Cabrita et al., 2020; Helmink et al., 2020; Petitprez et al., 2020; Sharonov et al., 2020). Formation of intratumoral TLSs improve the response to ICIs and increase the survival of cancer patients (Cabrita et al., 2020; Helmink et al., 2020; Petitprez et al., 2020; Sharonov et al., 2020). Given the synergistic anti-tumor immune response by NP-G2–044 + anti-PD-1 antibody, we investigated whether the combination therapy increased the number of intratumoral TLSs. We quantified the numbers of TLSs in tumor tissues from the four groups of mice, namely, control, NP-G2–044-treated, anti-PD-1-antibody-treated, and the combination (NP-G2–044 + anti-PD-1 antibody)-treated groups. TLSs were defined as a B220^{+} B cell follicle juxtaposed to a CD4^{+} T cell aggregate containing at least one CD21^{+} follicular DC (Helmink et al., 2020; Petitprez et al., 2020; Sharonov et al., 2020). The number of TLSs per mm^2 of tumor tissues and the ratio of TLSs to tumor area were counted and quantified using both 4T1 breast tumor and LLC lung cancer mouse models (Figures S6A–S6D). The combination treatment with NP-G2–044 + anti-PD-1 antibody increased the number of intratumoral TLSs and the ratio of TLSs to the tumor area (Figures S6A–S6E). These data are consistent with the fact that NP-G2–044 can improve the anti-tumor immune response to ICIs.

IL-12 and IFN-γ are necessary for the anti-tumor effect of the combination therapy of NP-G2–044 and anti-PD-1 antibody

Recently, it has been demonstrated that effective anti-PD-1 therapy requires intratumoral DCs producing interleukin-12 (IL-12) that stimulates anti-tumor CD8^{+} T cell immunity (Garris et al., 2018). In a positive feedback, anti-PD-1-activated CD8^{+} T cells release interferon gamma (IFN-γ) that can further activate intratumoral DCs. This crosstalk between intratumoral DCs and T cells (not observed in the local draining lymph node) is essential for an effective anti-PD-1 cancer immunotherapy (Garris et al., 2018). In the anti-PD-1-antibody-treated mice, there was an accumulation of IL-12-expressing DCs within the TME (Garris et al., 2018). This population of IL-12-expressing DCs uniquely expressed fascin (Garris et al., 2018). To investigate whether IL-12 and IFN-γ contribute to the NP-G2–044 + anti-PD-1 anti-tumor effect, we used neutralizing anti-IL-12 and anti-IFN-γ monoclonal antibodies (Figure 7). The protein levels of IL-12 and IFN-γ in the tumor tissues were increased by the combination treatment of NP-G2–044 + anti-PD-1 antibody (Figures 7A–7C and S7). Furthermore, mice in which IL-12 or IFN-γ or both were neutralized abolished the increase of overall survival by NP-G2–044 + anti-PD-1 antibody (Figures 7D and 7E). On the other hand, mice in which CSF1R was neutralized (to deplete macrophages) still generated the anti-tumor response by NP-G2–044 + anti-PD-1 antibody (Figures 7D and 7E). Collectively, these data indicate that IL-12 and IFN-γ are necessary for achieving the anti-tumor response, whereas macrophages may not be essential for the anti-tumor effect by NP-G2–044 + anti-PD-1 antibody. These data support the crosstalk of DCs and T cells in NP-G2–044 and anti-PD-1 anti-tumor immunotherapies.

DISCUSSION

A unique subset of fascin-high intratumoral DCs in human and mouse tumor tissues

In recent years, single-cell RNA sequencing (scRNA-seq) studies of cancer patient tumor tissue samples have provided an unprecedented view of the TME. There is a new and unique subset of DCs that have been observed in cancer patient's TME; this subset of intratumoral DCs have high fascin levels (Maier et al., 2020; Qian et al., 2020; Zhang et al., 2019; Zilionis et al., 2019). In one scRNA-seq analysis of NSCLC patients, increased expression levels of fascin were identified in DCs from tumor tissues compared with those of matched non-tumor lung tissues (Maier et al., 2020). These authors named these fascin-high intratumoral DCs mregDCs (mature DCs enriched in immunoregulatory molecules) (Maier et al., 2020). In addition to fascin, this subset of DCs also expressed high levels of CCR7, CCL19, LAMP3, and CCL22 (Maier et al., 2020). Both cDC1 and cDC2 cells could differentiate into mregDCs (Maier et al., 2020). Furthermore, in a comparative scRNA-seq study of colorectal, lung, ovarian, and breast cancers with tumor and matched normal tissues, fascin expression was found to be elevated in intratumoral DCs compared to that of other types of tumor-infiltrating immune cells (such as T cells, B cells, monocytes, macrophages, and neutrophils), endothelial cells, and fibroblasts (Qian et al., 2020). These intratumoral DCs could be subclassified into five DC phenotypes based on their transcriptomes (cDC1, cDC2, migratory cDCs, plasmacytoid DCs, and Langerhans-like DCs) (Qian et al., 2020). Fascin is highly expressed in the migratory cDCs that also express high levels of CCR7, CCL17, CCL19, and CCL22 (Qian et al., 2020). The number of migratory cDCs was increased in the tumor tissues compared with the matched normal tissues (Qian et al., 2020). Moreover, in a hepatocellular carcinoma scRNA-seq study, there were three enriched DC subsets identified within the TME, namely, cDC1, cDC2, and LAMP3^{+} DCs (Zhang et al., 2019). The LAMP3^{+} DCs highly expressed LAMP3, fascin, CD80, CD83, CCR7, and CCL19 (Zhang et al., 2019). The fraction of LAMP3^{+} DCs (arising from cDCs) in tumors was higher than that in adjacent liver tissues (Zhang et al., 2019). Additionally, in another scRNA-seq study of tumor tissue samples from NSCLC patients, the following four distinct subsets of intratumoral DCs were identified: cDC1, cDC2, pDC, and "activated" DC (Zilionis et al., 2019). The activated DCs were characterized by high fascin expression levels, as well as LAMP3, CCL19, CCR7, CCL22 (Zilionis et al., 2019). High fascin levels defined this subset of activated DCs in both human and mouse lung tumor tissues (Zilionis et al., 2019). Given the shared elevated expression of fascin, CCR7, CCL19, CCL22, and LAMP3, the above mregDCs, migratory DCs, LAMP3^{+} DCs, and activated DCs identified by these different research groups might be the same or overlapping DCs. Similar fascin-high intratumoral DCs were also observed in mouse tumor tissue samples (Garris et al., 2018; Maier et al., 2020; Zilionis et al., 2019; our current study).

Activation of fascin-high intratumoral DCs enhances the anti-tumor immune response of anti-PD-1 antibody

Our data show that activation of the fascin-high intratumoral DCs by NP-G2–044 can enhance the responses to anti-PD-1 antibody; this finding is consistent with previous reports (Garris et al., 2018; Maier et al., 2020). Activation of the mregDCs (fascin-high) by an IL-4

blocking antibody enhanced T cell effector function and anti-tumor activity (Maier et al., 2020). Activation of the IL-12-producing (fascin-high) DCs with agonistic CD40 monoclonal antibody also increased the anti-tumor activity of anti-PD-1 in an IL-12-dependent manner (Garris et al., 2018). These fascin-high intratumoral DCs are mature DCs because they express mature DC marker proteins, such as fascin and LAMP3, and possess the ability to migrate, likely in response to chemokines and chemokine receptors (such as CCL19, CCL22, and CCR7). Maturation is crucial for DC's ability to promote clonal expansion of antigen-specific T cells. This subset of DCs has already taken up the tumor antigens (becoming matured DCs) and is capable of activating T cells in the TME, as well as migrating to the draining lymph nodes to initiate T cell activation (Garris et al., 2018; Maier et al., 2020). Yet, previous studies and our current study indicate that activation of this subset of fascin-high intratumoral DCs could function synergistically with anti-PD-1 antibody to activate CD8^{+} T cells (Garris et al., 2018; Maier et al., 2020). Why does this subset of mature and activated DCs need to be activated to act with anti-PD-1 antibody? A possible analogy might be the exhausted T cells. This subset of fascin-high intratumoral DCs might be exhausted DCs (i.e., with reduced expression of cytokines, such as IL-12) and needs to be re-activated (or releasing the suppression). Furthermore, these fascin-high intratumoral DCs express the highest number of ligands to interact with receptors expressed on T cells and NK cells, thus likely the most active immune regulators of lymphocytes within the TME (Zhang et al., 2019). However, there is a strong correlation between this subset of DCs and the exhausted CD8^{+} T cell and Treg cell signature within the TME, implying that this subset of intratumoral DCs might be related to T cell dysfunction, despite their maturation features (Zhang et al., 2019). Moreover, the ability to expand antigen-specific CD8^{+} T cells is a feature of specialized effector DCs at early stages of maturation, and it is suppressed in exhausted DCs at late stages of maturation and in DCs matured under the conditions of chronic inflammation (Abdi et al., 2012; Carstensen et al., 2019; Rodrigue-Gervais et al., 2010). Long-term activation of DCs under conditions of chronic inflammation and cancer impairs their functionality, and a lack of IL-12 secretion results in non-functional T cells devoid of IFN-γ (Carstensen et al., 2019). Fascin inhibition, IL-4 inhibition, and CD40 activation, together with anti-PD-1 antibody, could release the inhibition and re-activate these DCs (Garris et al., 2018; Maier et al., 2020; this study). Because immature DCs express no or low levels of fascin, fascin inhibitors would not affect the migration of immature DCs into the tumor tissues (Bros et al., 2003; Ross et al., 2003; Yamashiro, 2012). Given that high expression levels of fascin have been observed in intratumoral DCs in cancer patients and that activation of these fascin-high DCs can enhance the anti-tumor immune response of anti-PD-1 antibody (Garris et al., 2018; Maier et al., 2020; this study), it is possible that targeting these intratumoral fascin-high DCs could enhance the anti-tumor response of anti-PD-1 immunotherapies to benefit cancer patients.

STAR★METHODS

RESOURCE AVAILABILITY

Lead contact—Further information and requests for reagents may be directed to and will be fulfilled by the Lead Contact, Xin-Yun Huang (xyhuang@med.cornell.edu).

Materials availability—All unique reagents generated in this study will be made available on request by the Lead Contact with a completed Materials Transfer Agreement (MTA).

Data and code availability—The published article includes all datasets generated or analyzed during this study.

EXPERIMENTAL MODEL AND SUBJECT DETAILS

Animal strains—BALB/c mice (female or male 6- to 8-week-old) were purchased from Charles River Labs. C57BL/6, and *Batf3*$^{-/-}$ mice (female 6- to 8 week-old) were purchased from the Jackson Laboratory. Studies using mice were performed in compliance with the Institutional Animal Care and Use Committee of Weill Medical College of Cornell University. All mice were housed in the facility of the Research Animal Resource Center of Weill Medical College of Cornell University.

Cell lines—Mouse 4T1 mammary tumor cells, mouse LLC lung cancer cells, and mouse PNEC30 prostate tumor cells were purchased from American Type Culture Collection. Fascin gene deleted LLC cells, mouse EMT6 mammary tumor cells, mouse Pan02 pancreatic tumor cells, mouse Hepa1–6 liver cancer cells, mouse Renca kidney cancer cells, and mouse cDC1 cells (MutuDC1 cells) were obtained from Drs. Shengyu Yang, Chenbo Zeng, David Lyden, David Cohen, Larry Gazda and Hans Acha-Orbea, respectively. These cells were cultured as previously described (Chen et al., 2010; Costa-Silva et al., 2015; Ersoy et al., 2018; Fuertes Marraco et al., 2012; Han et al., 2016; Huang et al., 2015; Martis et al., 2018; McDonald et al., 2017).

METHOD DETAILS

Breast cancer models—Female BALB/c mice (6- to 8-week-old) were purchased from Charles River. 4T1 tumor cells (5×10^4 or 1×10^5) were injected subcutaneously into the abdominal mammary gland area of mice using a single-cell suspension in PBS-matrigel (v/v, 1:1) on day 0 as previously described (Chen et al., 2010; Han et al., 2016; Huang et al., 2015; Shan et al., 2005; Yang et al., 2009, 2012). Lower numbers of 4T1 tumor cells were injected into each mouse in experiments presented in Figures 2A and 2B (5×10^4 cells), than in experiments presented in Figures 1A and 1B (1×10^5 cells). Starting on day 7, NP-G2–044 dissolved in PEG400 was given once a day for 5 days a week by gavage at 100 mg kg^{-1} per mouse. Control solvent was given to the control group of mice once a day for 5 days a week by gavage. 10 mg/kg anti–PD-1 antibody and /or anti–CTLA-4 antibody was given by i.p. on day 11, 13, 15, and 17 as previously described (Kim et al., 2014). Isotype control at equivalent doses was given to the control group of mice by i.p. on day 11, 13, 15, and 17. Primary tumor volume was calculated as length $\times$ width^2 $\times$ π/6. Death of mice was used as the endpoint for all the overall survival studies.

For other assays using 4T1 tumors (such as by FACS, mass spectrometry, and tertiary lymphoid structure (TLS) staining), 4T1 tumor cells (1×10^5) were injected subcutaneously into the abdominal mammary gland area of mice using a single-cell suspension in PBS-matrigel (v/v, 1:1) on day 0. Control solvent, NP-G2–044 and /or anti–PD-1 antibody dosing

was performed as in the overall survival studies. On day 23, the tumor tissues were dissected.

For EMT6 breast tumor mouse model, EMT6 tumor cells (1×10^5) were injected subcutaneously into the abdominal mammary gland area of female BALB/c mice (6- to 8-week-old) using a single-cell suspension in PBS-matrigel (v/v, 1:1) on day 0. Starting on day 14, NP-G2–044 was given to mice once a day for 5 days a week by gavage at 100 mg kg^{-1} per mouse. Control solvent was given to the control group of mice once a day for 5 days a week by gavage. 10 mg/kg anti–PD-1 and anti–CTLA-4 antibodies were given by i.p. on day 11, 13, 15, and 17 as previously described (Kim et al., 2014). Primary tumor volume was calculated as length × width^2 × π/6.

Lung cancer model—Female C57BL/6 mice (6- to 8-week-old) and B6.129S(C)-Batf3 tm1Kmm/J mice (6- to 8-week-old) were purchased from The Jackson Laboratory. Wild-type or fascin knock out LLC tumor cells (1×10^5) suspended in PBS were injected into the lung of mice on day 0. Starting on day 5, NP-G2–044 was given to mice once a day for 4 days a week by gavage at 50 mg/kg per mouse. Control solvent was given to the control group of mice once a day for 4 days a week by gavage. 10 mg/kg anti–PD-1 or anti-PD-1 + anti–CTLA-4 antibodies were given by i.p. on day 6, 8, 10, and 12. Death of mice was used as the endpoint for all the overall survival studies.

For IL-12 and IFN-γ studies, LLC tumor cells (1×10^5) suspended in PBS were injected into the lung of mice on day 0. Starting on day 5, NP-G2–044 was given to mice once a day for 4 days a week by gavage at 50 mg/kg per mouse. Control solvent was given to the control group of mice once a day for 4 days a week by gavage. 10 mg/kg anti–PD-1 antibodies were given by i.p. on day 6, 8, 10, and 12. Anti-IL-12p40 or anti-IFN-γ or anti-CSF1R antibody dosing was performed as previously described (Garris et al., 2018; Glasner et al., 2018; Moynihan et al., 2016). Starting on day 4, mice were dosed by i.p. with 500 μg of anti-IL-12p40 for 5 times in the following week and/or injected i.p. twice a week with 200 μg of anti-IFN-γ, or dosed by i.p. with 300 μg of anti-CSF1R three times a week (n = 5).

For immune cell isolations from tumor tissues, LLC tumor cells (2.5×10^4) suspended in PBS were injected into the lungs of mice on day 0. Control solvent, NP-G2–044 and /or anti–PD-1 antibody dosing was performed as in overall survival studies. On day 26, the tumor tissues were dissected for immune cell isolations.

For TLS staining and relative fluorescence intensity detection of IL-12 and IFN-γ, LLC tumor cells (2.5×10^4) suspended in PBS were injected into the lungs of mice on day 0. Control solvent, NP-G2–044 and /or anti–PD-1 antibody dosing was performed as in overall survival studies. On day 23, the tumor tissues were dissected for frozen section preparation.

Pancreatic cancer model—Female C57BL/6 mice (6- to 8-week-old) were purchased from The Jackson Laboratory. Pan02 tumor cells (1×10^5) suspended in PBS were injected into the spleen of mice on day 0, starting on day 4, NP-G2–044 was given to mice once a day for 4 days a week by gavage at 50 mg kg^{-1} per mouse. Control solvent was given to the

control group of mice once a day for 4 days a week by gavage. 10 mg/kg anti–PD-1 and anti–CTLA-4 antibodies were given by i.p. on day 3, 6, 9, and 12. Death of mice was used as the endpoint for all the overall survival studies.

Prostate cancer model—Male BALB/c mice (6- to 8-week-old) were purchased from Charles River. PNEC30 tumor cells (6×10^5) suspended in PBS were injected into the prostate of mice on day 0. Starting on day 7, NP-G2–044 was given to mice once a day for 5 days a week by gavage at 100 mg kg^{-1} per mouse. Control solvent was given to the control group of mice once a day for 5 days a week by gavage. 10 mg/kg anti–PD-1 and anti–CTLA-4 antibodies were given by i.p. on day 11, 13, 15, and 17. Death of mice was used as the endpoint for all the overall survival studies.

Liver cancer model—Female C57BL/6 mice (6- to 8-week-old) were purchased from The Jackson Laboratory. Hepa 1–6 tumor cells (3×10^6) suspended in PBS were injected into the left lobes of the liver of mice on day 0. Starting on day 7, NP-G2–044 was given to mice once a day for 4 days a week by gavage at 50 mg kg^{-1} per mouse. Control solvent was given to the control group of mice once a day for 4 days a week by gavage. 10 mg/kg anti–PD-1 antibody was given by i.p. on day 11, 13, 15, and 17. Death of mice was used as the endpoint for all the overall survival studies.

Kidney cancer model—Male BALB/c mice (6- to 8-week-old) were purchased from Charles River. Renca tumor cells (1×10^6) suspended in PBS were injected into the center of the left kidney of mice on day 0. Starting on day 14, NP-G2–044 was given to mice once a day for 5 days a week by gavage at 100 mg kg^{-1} per mouse. Control solvent was given to the control group of mice once a day for 5 days a week by gavage. 10 mg/kg anti–PD-1 antibody was given by i.p. on day 11, 13, 15, and 17. Death of mice was used as the endpoint for all the overall survival studies.

Immune cell isolation from tissues—To profile lymphoid cells, single-cell suspensions were prepared from lymph nodes and spleens by tissue disruption with glass slides. The dissociated cells were passed through 70 μm filters and pelleted. To profile myeloid cells from lymph nodes and spleens, tissues were mechanically disrupted with a razor blade, then incubated in 300 U/ml Collagenase Type 3 (Worthington Biochemicals) in RPMI supplemented with 10% FBS for 35 min at 37°C. EDTA was added for final concentration of 0.01 M, incubated for 5 min at 37°C, then 5 min on ice, then cells were passed through 70 μm filter for single cells suspension and downstream flow cytometric analysis. Primary tumor tissues were harvested, weighted, minced with a razor blade, and then digested in 280 U/ml Collagenase Type 3 and 4 mg/ml DNase I (Sigma) in HBSS at 37°C for 1 h with periodic vortex every 20 min. Digested tissues were passed through 70 μm filters and pelleted. Cells were resuspended in 40% Percoll (Sigma) and layered above 60% Percoll. Sample was centrifuged at 1,900 g at 4°C for 30 min without brake. Cells at interface were collected, stained and analyzed by flow cytometry or used for sorting.

Flow cytometry—Antibodies against CD45 (Cat#64-0451-82, clone 30-F11), CD4 (Cat#78-0048-12, clone GK1.5), CD25 (Cat#45-0251-82 clone PC61.5), CD31 (Cat#25-0311-81, clone 390), CD140a (Cat#17-1401-81, clone APA5), Foxp3

(Cat#48-5773-80, clone FJK-16 s), Ki67 (Cat#41-5698-80, SolA15), NKp46 (Cat#11-3351-82, clone 29A1.4) and PD-L1 (Cat#25-5982-82, clone MIH5) were purchased from eBioscience. Antibodies against B220 (Cat#13-0452-82,clone RA3–6B2), CD11b (Cat#67-0112-82,clone M1–70), CD11c (Cat#48-0114-82, clone N418), CD8 (Cat#100741, clone 53–6.7), CD40 (Cat#102912, clone HM40–3), CD80 (Cat#104810, clone 16–10A1), CD86 (Cat#105012, clone GL-1), Ly6C (Cat#128026, clone HK1.4), Ly6G (Cat# 217618,clone 1A8), MHC II (Cat#107639, clone M5/114.15.2), PD-1 (Cat#109109, clone RMP1–30), TCRb (Cat#109241, clone H57–597), XCR1 (Cat#148210, clone ZET), CD172a (Cat#144014, clone P84) were purchased from Biolegend. Antibody against Granzyme B (Cat# GBR05, clone GB11) was from Invitrogen. Fascin (Cat#sc-46675PE, clone D-10) was purchased from Santa Cruz Biotechnology. All antibodies were tested with their isotype controls. After 20 min incubation with Zombie UV™ Fixable stain at room temperature, all samples were washed with BD FACS buffer and stained with the appropriate surface antibodies. Cell-surface staining was conducted by incubating cells with antibodies for 30 min on ice in the presence of 2.4G2 mAb to block FcγR binding. Markers used for various cell types were: CD8$^+$ T cells (live CD45$^+$Nkp46$^-$TCRβ$^+$ CD8$^+$), conventional CD4$^+$Foxp3$^-$ T cells (live CD45$^+$Nkp46$^-$TCRβ$^+$CD4$^+$), Treg cells (live CD45$^+$Nkp46$^-$TCRβ$^+$CD4$^+$Foxp3$^+$), B cells (live CD45$^+$B220+), NK cells (live CD45$^+$Nkp46$^+$TCRβ$^-$), cDC1 cells (live CD45$^+$F4/80$^-$MHC$^+$CD11c$^+$XCR1$^+$), cDC2 cells (live CD45$^+$F4/80$^-$MHC$^+$CD11c$^+$CD172a$^+$), TAMs (live CD45$^+$F4/80$^+$CD11b$^+$Ly6C$^-$Ly6G$^-$), G-MDSCs (live CD45$^+$CD11b$^+$Ly6C$^-$Ly6G$^+$), M-MDSCs (live CD45$^+$CD11b$^+$Ly6C$^+$ly6G$^-$), ECs (live CD45$^-$CD31$^+$), and CAFs (live CD45$^-$FAP$^+$). Intracellular staining for Foxp3 (FJK-16 s), Ki67 (SolA15), Granzyme B (GB11), and fascin (D-10) was performed according to Foxp3/Transcription Factor Staining buffer set (eBioscience). Data acquisition was performed on FACSCabibur (BC Biosciences) or FACS LSRII (Becton Dickinson), and analyzed via FlowJo software (Tree Star, Inc.).

Generation of fascin knockout LLC cells—Fascin targeting sequences (sgRNA, TCGCTACCTGGCCGCCGACA) were inserted LentiCRISPRv2 to generate LentiCRISPRv2-fascin plasmid (Lin et al., 2019). LLC cells were transfected with LentiCRISPRv2-fascin using LIPO3000 (ThermoFisher) according to the manufacturer's instructions. Media was changed 24 hr post transfection and cells were selected using 5 µg/mL of puromycin for 96 hr post transfection. Individual clones containing the fascin knockout cells were then generated by plating the transfected cells at a density of 0.5 cells per well into three 96-well plates. Wells containing a single cell were identified 24 hr after plating. Fascin expression detection by anti-fascin 1 antibody through western blotting was used to confirm the fascin knockout.

Lentivirus generation—Lentiviruses were produced by co-transfection of 293T cells with psPAX2, pMDG2, and MISSION pLKO.1-puro Empty Vector or FSCN1 MISSION shRNA (TRCN0000335363, Sigma) with lipofectamine 3000 (Life Technologies). Virus supernatants collected 48 hr and 72 hr post transfection were combined, centrifuged at 2,000 rpm for 10 min to remove cellular debris. Lentiviral supernatants were filtered with 0.45 µm pore filters and harvested.

Bone marrow derived dendritic cell (BMDCs) generation and lentivirus transduction—Murine bone marrow was flushed from femur and tibiae of C57BL/6 mice, and then passed through 40 μm filter to achieve single cell suspension. After red blood cell lysis, Progenitors were washed and plated with 5×10^6 cells in complete media (RMPI-1640 supplemented with 10% heat-inactivated FBS, 100 U/ml penicillin and streptomycin (P/S), 2 mM L-glutamine, and 1 mM sodium pyruvate) with 20 ng/ml GM-CSF (R&D) and 20 ng/ml IL4 (R&D) for 3 days. On day 4, immature DCs were transduced with pLKO.1-puro empty vector or fascin-shRNA containing lentivirus using 10 μg/ml polybrene (Santa Cruz). After 16 hr incubation, viruses were removed and replaced with fresh complete media supplemented with 20 ng/ml GM-CSF and 20 ng/ml IL4. On day 6, BMDCs were treated with 2 μg/ml puromycin for 2 days and harvested for fascin knockdown verification by western blotting or functional assay on day 8.

BMDCs adoptive transfer—For adoptive transfer, CD11c$^+$ cells were depleted in bone marrow harvested from C57BL/6 donors using CD11c MicroBeads UltraPure (Miltenyi Biotec). 2.5×10^6 pLKO.1-puro empty vector or fascin-knocking down BMDCs were mixed with 2.5×10^6 CD11c$^+$ cell-depleted bone marrow and then intravenously injected into recipient mouse one the same day after 899 cGy total body irradiation from a ^{137}Cs source. On the 8th day after bone marrow transplantation, LLC tumor cells (1×10^5) suspended in PBS were injected into the lungs of the recipients. The following dosing of NP-G2–044 and/or anti–PD-1 was performed like the above LLC tumor models for overall survival studies. All animal survival curves were depicted by Stata 7.

Cell migration assay—Dendritic cell migration assay was conducted according to a modified method as previously described (Van Goethem et al., 2010). Briefly, Type I Atelo-Collagen (2 mg/ml final concentrations, Advanced BioMatrix) was loaded onto Transwell inserts and allowed to polymerize for 30 min in an incubator at 37°C. Neutralization of the fibrillar collagen I matrix was conducted by rehydration of the matrix with 500 μL warm culture medium for 3 h in the incubator at 37°C with 5% CO_2 before seeding the cells. 2×10^5 spleen-derived dendritic cells suspended in 200 μl starvation medium with 0.02% FBS were added to the upper chamber of an insert (Falcon), and the insert was placed in a 24-well plate containing 500 μl starvation medium with 20% FBS. When used, PEG400 or NP-G2–044 (1, 3, 10, or 30 μM final concentrations) were added to both the upper and the lower chambers. Migration assays were performed for 8 h and cells were fixed with 10% paraformaldehyde. Cells were stained with crystal violet staining solution, and cells on the upper side of the insert were removed with a cotton swab. The whole fields on the lower side of the insert were scanned, and the migrated cells were counted by ImageJ.

For LLC cell migration, 1×10^5 or 2×10^5 LLC wild-type or fascin knock-out cells suspended in 200 μl starvation medium (DMEM) were added to the upper chamber of an insert (Falcon), respectively, as previously described (Huang et al., 2015). Insert was placed in a 24-well plate containing 500 μl starvation medium with 10% FBS. When used, PEG 400 or NP-G2–044 (30 μM final concentrations) was added to both the upper and the lower chambers (n = 3). Migration assays were performed for 24 hr and cells were fixed with 10% paraformaldehyde. Cells were stained with crystal violet staining solution, and cells on the

upper side of the insert were removed with a cotton swab. The whole fields on the lower side of the insert were scanned, and the migrated cells were counted by ImageJ.

Dendritic cell antigen uptake assay—The quantification of antigen (BSA or Dextran) uptake by dendritic cells was performed using a previously described protocol (Hodakoski et al., 2019). cDC1 (MutuDC1) cells were plated in 12-well plates containing glass coverslips (Smita et al., 2018). After 24 hr of attachment, cells were incubated in serum-free medium for 16 hr. Cells were incubated in serum-free medium by addition of 10 μM (for Dextran treatment) or 3 μM NP-G2–044 (for BSA treatment) or dissolvent (PEG 400) for 5 h, followed by addition of 0.5 mg/ml Cascade Blue™ Dextran (D7132, Thermo Fisher)(MW: 3000) or 0.5 mg/ml Alexa Fluor 488 BSA (A13100, Thermo Fisher)(MW: 66,000) for 1 h, respectively. Cells were washed with ice-cold PBS 3 times, followed by one wash with a low pH buffer (0.1 M sodium acetate, 0.05 M NaCl, pH 5.5) to bleach surface bound Dextran or two more ice-cold PBS wash, respectively. Cells were then fixed with 4.0% paraformaldehyde in PBS for 10 min at room temperature, and then washed twice with PBS. Cells were incubated for 10 min at room temperature with PBS containing 0.5% Triton X-100. After 3 times PBS wash, cells were blocked by 1.0% BSA in PBST (PBS+ 0.1% Tween 20) for 30 min. Cells were incubated in the diluted anti-vinculin antibody (Santa Cruz Biotechnology) in 1.0% BSA in PBST in a humidified chamber for 1 h at room temperature. After 3 times PBS wash, cells were incubated with the secondary antibody, Rhodamine (TRITC) AffiniPure Donkey Anti-Goat IgG (H+L) (Jackson ImmunoResearch Inc), in 1.0% BSA in PBST for 1 h at room temperature in the dark, followed by 3 times wash with PBS in the dark. Cells were stained by Alexa Fluor 488 Phalloidin (Invitrogen) or DAPI for 20 min or 10 min, respectively. After 3 times PBS wash, cells were mounted on glass slides. Images were acquired with a LSM880 with Airyscan and FAST Airyscan High Resolution and 32-channel spectral Detectors Microscope. Vinculin-positive cells were counted under microscope for six randomly selected view fields. Uptake of fluorescently labeled Dextran or BSA was quantified according to a modified method (Commisso et al., 2014). Macropinocytic index was determined by calculating the total area of internalized fluorescent Dextran or BSA normalized to the total area of cells or nuclei, respectively.

For antigen uptake assays *in vivo*, GFP-expressing 4T1 cells were generated by retroviral transduction with pBMN-IRES-GFP. GFP-labeled 4T1 tumor cells (5×10^5) were injected subcutaneously into the abdominal mammary gland area of mice using a single-cell suspension in PBS-matrigel (v/v, 1:1) on day 0 as previously described (Chen et al., 2010; Han et al., 2016; Huang et al., 2015; Shan et al., 2005; Yang et al., 2009). Starting on day 7, NP-G2–044 dissolved in PEG400 was given once a day for 5 days a week by gavage at 100 mg kg^{-1} per mouse. Control solvent was also given to the control group of mice once a day for 5 days a week by gavage. The tumor tissues were dissected for GFP$^+$ DC or macrophage detection by FACS on day 20. Antigen uptake by DCs or macrophages from GFP-labeled 4T1 tumor cells was quantified by GFP signal in DCs (CD45$^+$Siglec-F$^-$F4/80$^-$MHC$^+$CD11c$^+$) or macrophages (CD45$^+$Siglec-F$^-$F4/80$^+$MHC$^+$CD11c$^-$).

Immunofluorescence staining—Antibodies against XCR1 (ZET) and CD8a (53–6.7) were purchased from Biolegend. Antibody against Fascin (sc-46675AF647) was purchased

from Santa Cruz Biotechnology. Tumor tissues were frozen in O.C.T. medium (Sakura Finetek USA) and sectioned at the thickness of 10 μm. Tumor sections were fixed and stained with antibodies. Subsequently, they were mounted with VECTORSHIELD anti-fade mounting media (Vector Laboratories) and scanned by Pannoramic Digital Slide Scanners (3DHISTECH LTD). Immunofluorescence images were analyzed with CaseViewer software. Intensity was indicated by the lookup table shown in the individual figures using ImageJ.

Protein identification and quantitation by mass spectrometry—The tumor tissue samples (n = 3) were dissected on day 25, and digested in solution with trypsin overnight at 37°C following reduction with 5 mM DTT and alkylation with 14 mM iodoacetamide. The digests were vacuum centrifuged to near dryness and desalted by C18 Sep-Pak columns. A Thermo Fisher Scientific EASY-nLC 1000 coupled on-line to a Fusion Lumos mass spectrometer (Thermo Fisher Scientific) was used for LC-MS analysis. Buffer A (0.1% FA in water) and buffer B (0.1% FA in ACN) were used as mobile phases for gradient separation. A 75 μm × 15 cm chromatography column (ReproSil-Pur C18-AQ, 3 μm, Dr. Maisch GmbH, German) was packed in-house for peptides separation. Peptides were separated with a gradient of 3%–28% buffer B over 110 min, 28%–80% B over 10 min at a flow rate of 300 nL/min. The Fusion Lumos mass spectrometer was operated in data dependent mode. Full MS scans were acquired in the Orbitrap mass analyzer over a range of 300–1500 m/z with resolution 60,000 at m/z 200. The top 18 most abundant precursors with charge states between 2 and 6 were selected with an isolation window of 1.2 Thomsons and fragmented by higher-energy collisional dissociation with normalized collision energy of 35. MS/MS scans were acquired in the Orbitrap mass analyzer with resolution 15,000 at m/z 200. The automatic gain control target value was 5e5 for MS scans and 2e5 for MS/MS scans respectively, and the maximum ion injection time is 50 ms for both. The raw files were processed using the MaxQuant computational proteomics platform version 1.5.5.1 (Max Planck Institute, Munich, Germany) for protein identification (Cox and Mann, 2008). The fragmentation spectra were used to search the UniProt mouse protein database. Oxidation of methionine and protein N-terminal acetylation were used as variable modifications for database searching. The precursor and fragment mass tolerances were set to 7 and 20 ppm, respectively. Both peptide and protein identifications were filtered at 1% false discovery rate based on decoy search using a database with the protein sequences reversed. Relative protein quantitation was performed based on protein intensity values reported by MaxQuant. After LC/MS/MS analyses, the top ~180 proteins with the most significant changes (ranked by the *p* values) from treated group compared with the control group were analyzed using the STRING interaction network program and displayed using Cytoscape. The displayed network was with a combined confidence score of at least 0.400.

Tertiary lymphoid structure (TLS) staining—LLC or 4T1 tumor tissues were fixed in 2% paraformaldehyde (PFA) overnight, followed by embedding in optimum cutting temperature (O.C.T.; Tissue-Tek) compound, and were cut into 14-μm sections. The tumor tissue sections were then blocked with 1.0% BSA in PBST (PBS+ 0.1% Tween 20) and stained with fluorophore-conjugated CD4 (Biolegend), B220 (eBioscience) and CD21 (BD Biosciences) antibodies at room temperature for 3 h. The sections were counterstained with

DAPI and mounted on glass slides. Images were acquired with a LSM880 microscope with Airyscan and FAST Airyscan High Resolution and 32-channel spectral detectors.

Relative fluorescence intensity of IL-12 and IFN-γ—LLC tumor tissue sections were prepared as previously described (Oh et al., 2017). Briefly, tumor tissues were fixed in 2% paraformaldehyde overnight, followed by embedding in optimum cutting temperature (O.C.T.; Tissue-Tek) compound, and were cut into 14-μm sections. The sections were blocked with 1.0% BSA in PBST (PBS+ 0.1% Tween 20) and incubated with anti-mouse IL-12 p40 (Bio X Cell) or anti-mouse IFN-γ (Bio X Cell) at room temperature for 1 hr. After wash 3 times with PBST, the sections were stained with goat anti-rat IgG H&L (Alexa Fluor® 568) at room temperature for 1 hr. The sections were next counterstained with DAPI and mounted on glass slides. Images were acquired with a LSM880 microscope with Airyscan and FAST Airyscan High Resolution and 32-channel spectral detectors. Relative fluorescence intensity of IL-12 or IFN-γ was quantified by normalizing integrated fluorescence intensity of IL-12 or IFN-γ to the total cell numbers of macrophages, DCs, or $CD8^+$ T cells per mg of tumor.

QUANTIFICATION AND STATISTICAL ANALYSIS

In Figures 3, 4A–4D, 5B, 7A, and 7B, the assays were repeated three times, and the data are represented as mean ± SEM of the three independent experiments. ANOVA followed by the Dunnett's test, or Student's t test, was used for statistical analysis as indicated in the figure legends. Overall survival data analyses in Figures 1, 2, 5C, 5E, 5F, 7D, and 7E were performed with log-rank test. In all the figures, significant p values are identified as follows: *, $p < 0.05$; **, $p < 0.005$.

Supplementary Material

Refer to Web version on PubMed Central for supplementary material.

ACKNOWLEDGMENTS

DECLARATION OF INTERESTS

Novita Pharmaceuticals supported part of the work through a Sponsored Research Agreement. X.-Y.H. and J.J.Z. are co-founders and have equity in Novita Pharmaceuticals.

REFERENCES

Abdi K, Singh NJ, and Matzinger P (2012). Lipopolysaccharide-activated dendritic cells: "exhausted" or alert and waiting? J. Immunol 188, 5981–5989. [PubMed: 22561154]

Barry M, and Bleackley RC (2002). Cytotoxic T lymphocytes: all roads lead to death. Nat. Rev. Immunol 2, 401–409. [PubMed: 12093006]

Bros M, Ross XL, Pautz A, Reske-Kunz AB, and Ross R (2003). The human fascin gene promoter is highly active in mature dendritic cells due to a stage-specific enhancer. J. Immunol 171, 1825–1834. [PubMed: 12902483]

Bryan J, and Kane RE (1978). Separation and interaction of the major components of sea urchin actin gel. J. Mol. Biol 125, 207–224. [PubMed: 731692]

Cabrita R, Lauss M, Sanna A, Donia M, Skaarup Larsen M, Mitra S, Johansson I, Phung B, Harbst K, Vallon-Christersson J, et al. (2020). Tertiary lymphoid structures improve immunotherapy and survival in melanoma. Nature 577, 561–565. [PubMed: 31942071]

Carstensen LS, Lie-Andersen O, Obers A, Crowther MD, Svane IM, and Hansen M (2019). Long-Term Exposure to Inflammation Induces Differential Cytokine Patterns and Apoptosis in Dendritic Cells. Front. Immunol 10, 2702. [PubMed: 31824496]

Chabaud M, Heuzé ML, Bretou M, Vargas P, Maiuri P, Solanes P, Maurin M, Terriac E, Le Berre M, Lankar D, et al. (2015). Cell migration and antigen capture are antagonistic processes coupled by myosin II in dendritic cells. Nat. Commun 6, 7526. [PubMed: 26109323]

Chen DS, and Mellman I (2017). Elements of cancer immunity and the cancer-immune set point. Nature 541, 321–330. [PubMed: 28102259]

Chen L, Yang S, Jakoncic J, Zhang JJ, and Huang XY (2010). Migrastatin analogues target fascin to block tumour metastasis. Nature 464, 1062–1066. [PubMed: 20393565]

Commisso C, Flinn RJ, and Bar-Sagi D (2014). Determining the macropinocytic index of cells through a quantitative image-based assay. Nat. Protoc 9, 182–192. [PubMed: 24385148]

Costa-Silva B, Aiello NM, Ocean AJ, Singh S, Zhang H, Thakur BK, Becker A, Hoshino A, Mark MT, Molina H, et al. (2015). Pancreatic cancer exosomes initiate pre-metastatic niche formation in the liver. Nat. Cell Biol 17, 816–826. [PubMed: 25985394]

Cox J, and Mann M (2008). MaxQuant enables high peptide identification rates, individualized p.p.b.-range mass accuracies and proteome-wide protein quantification. Nat. Biotechnol 26, 1367–1372. [PubMed: 19029910]

DuPré SA, Redelman D, and Hunter KW Jr. (2007). The mouse mammary carcinoma 4T1: characterization of the cellular landscape of primary tumours and metastatic tumour foci. Int. J. Exp. Pathol 88, 351–360.

Elkhatib N, Neu MB, Zensen C, Schmoller KM, Louvard D, Bausch AR, Betz T, and Vignjevic DM (2014). Fascin plays a role in stress fiber organization and focal adhesion disassembly. Curr. Biol 24, 1492–1499. [PubMed: 24930964]

Ersoy BA, Maner-Smith KM, Li Y, Alpertunga I, and Cohen DE (2018). Thioesterase-mediated control of cellular calcium homeostasis enables hepatic ER stress. J. Clin. Invest 128, 141–156. [PubMed: 29202465]

Fuertes Marraco SA, Grosjean F, Duval A, Rosa M, Lavanchy C, Ashok D, Haller S, Otten LA, Steiner QG, Descombes P, et al. (2012). Novel murine dendritic cell lines: a powerful auxiliary tool for dendritic cell research. Front. Immunol 3, 331. [PubMed: 23162549]

Garris CS, Arlauckas SP, Kohler RH, Trefny MP, Garren S, Piot C, Engblom C, Pfirschke C, Siwicki M, Gungabeesoon J, et al. (2018). Successful Anti-PD-1 Cancer Immunotherapy Requires T Cell-Dendritic Cell Crosstalk Involving the Cytokines IFN-γ and IL-12. Immunity 49, 1148–1161.e7. [PubMed: 30552023]

Gimona M, Buccione R, Courtneidge SA, and Linder S (2008). Assembly and biological role of podosomes and invadopodia. Curr. Opin. Cell Biol 20, 235–241. [PubMed: 18337078]

Glasner A, Levi A, Enk J, Isaacson B, Viukov S, Orlanski S, Scope A, Neuman T, Enk CD, Hanna JH, et al. (2018). NKp46 Receptor-Mediated Interferon-γ Production by Natural Killer Cells Increases Fibronectin 1 to Alter Tumor Architecture and Control Metastasis. Immunity 48, 396–398.

Grothey A, Hashizume R, Sahin AA, and McCrea PD (2000). Fascin, an actin-bundling protein associated with cell motility, is upregulated in hormone receptor negative breast cancer. Br. J. Cancer 83, 870–873. [PubMed: 10970687]

Han S, Huang J, Liu B, Xing B, Bordeleau F, Reinhart-King CA, Li W, Zhang JJ, and Huang XY (2016). Improving fascin inhibitors to block tumor cell migration and metastasis. Mol. Oncol 10, 966–980. [PubMed: 27071719]

Hashimoto Y, Skacel M, and Adams JC (2005). Roles of fascin in human carcinoma motility and signaling: prospects for a novel biomarker? Int. J. Biochem. Cell Biol 37, 1787–1804. [PubMed: 16002322]

Hashimoto Y, Kim DJ, and Adams JC (2011). The roles of fascins in health and disease. J. Pathol 224, 289–300. [PubMed: 21618240]

Helmink BA, Reddy SM, Gao J, Zhang S, Basar R, Thakur R, Yizhak K, Sade-Feldman M, Blando J, Han G, et al. (2020). B cells and tertiary lymphoid structures promote immunotherapy response. Nature 577, 549–555. [PubMed: 31942075]

Hildner K, Edelson BT, Purtha WE, Diamond M, Matsushita H, Kohyama M, Calderon B, Schraml BU, Unanue ER, Diamond MS, et al. (2008). Batf3 deficiency reveals a critical role for CD8alpha + dendritic cells in cytotoxic T cell immunity. Science 322, 1097–1100. [PubMed: 19008445]

Hodakoski C, Hopkins BD, Zhang G, Su T, Cheng Z, Morris R, Rhee KY, Goncalves MD, and Cantley LC (2019). Rac-Mediated Macropinocytosis of Extracellular Protein Promotes Glucose Independence in Non-Small Cell Lung Cancer. Cancers (Basel) 11, 37.

Huang FK, Han S, Xing B, Huang J, Liu B, Bordeleau F, Reinhart-King CA, Zhang JJ, and Huang XY (2015). Targeted inhibition of fascin function blocks tumour invasion and metastatic colonization. Nat. Commun 6, 7465. [PubMed: 26081695]

Huang J, Dey R, Wang Y, Jakoncic J, Kurinov I, and Huang XY (2018). Structural Insights into the Induced-fit Inhibition of Fascin by a Small-Molecule Inhibitor. J. Mol. Biol 430, 1324–1335. [PubMed: 29573988]

Kim K, Skora AD, Li Z, Liu Q, Tam AJ, Blosser RL, Diaz LA Jr., Papadopoulos N, Kinzler KW, Vogelstein B, and Zhou S (2014). Eradication of metastatic mouse cancers resistant to immune checkpoint blockade by suppression of myeloid-derived cells. Proc. Natl. Acad. Sci. USA 111, 11774–11779. [PubMed: 25071169]

Li A, Morton JP, Ma Y, Karim SA, Zhou Y, Faller WJ, Woodham EF, Morris HT, Stevenson RP, Juin A, et al. (2014). Fascin is regulated by slug, promotes progression of pancreatic cancer in mice, and is associated with patient outcomes. Gastroenterology 146, 1386–1396.e1–17. [PubMed: 24462734]

Lin S, Huang C, Gunda V, Sun J, Chellappan SP, Li Z, Izumi V, Fang B, Koomen J, Singh PK, et al. (2019). Fascin Controls Metastatic Colonization and Mitochondrial Oxidative Phosphorylation by Remodeling Mitochondrial Actin Filaments. Cell Rep. 28, 2824–2836.e8. [PubMed: 31509745]

Maier B, Leader AM, Chen ST, Tung N, Chang C, LeBerichel J, Chudnovskiy A, Maskey S, Walker L, Finnigan JP, et al. (2020). A conserved dendritic-cell regulatory program limits antitumour immunity. Nature 580, 257–262. [PubMed: 32269339]

Martis PC, Dudley AT, Bemrose MA, Gazda HL, Smith BH, and Gazda LS (2018). MEF2 plays a significant role in the tumor inhibitory mechanism of encapsulated RENCA cells via EGF receptor signaling in target tumor cells. BMC Cancer 18, 1217. [PubMed: 30514247]

Mattila PK, and Lappalainen P (2008). Filopodia: molecular architecture and cellular functions. Nat. Rev. Mol. Cell Biol 9, 446–454. [PubMed: 18464790]

McDonald ES, Mankoff J, Makvandi M, Chu W, Chu Y, Mach RH, and Zeng C (2017). Sigma-2 ligands and PARP inhibitors synergistically trigger cell death in breast cancer cells. Biochem. Biophys. Res. Commun 486, 788–795. [PubMed: 28347815]

Mellman I, and Steinman RM (2001). Dendritic cells: specialized and regulated antigen processing machines. Cell 106, 255–258. [PubMed: 11509172]

Moynihan KD, Opel CF, Szeto GL, Tzeng A, Zhu EF, Engreitz JM, Williams RT, Rakhra K, Zhang MH, Rothschilds AM, et al. (2016). Eradication of large established tumors in mice by combination immunotherapy that engages innate and adaptive immune responses. Nat. Med 22, 1402–1410. [PubMed: 27775706]

Oh SA, Liu M, Nixon BG, Kang D, Toure A, Bivona M, and Li MO (2017). Foxp3-independent mechanism by which TGF-β controls peripheral T cell tolerance. Proc. Natl. Acad. Sci. USA 114, E7536–E7544. [PubMed: 28827353]

Ott PA, Hodi FS, Kaufman HL, Wigginton JM, and Wolchok JD (2017). Combination immunotherapy: a road map. J. Immunother. Cancer 5, 16. [PubMed: 28239469]

Otto JJ, Kane RE, and Bryan J (1979). Formation of filopodia in coelomocytes: localization of fascin, a 58,000 dalton actin cross-linking protein. Cell 17, 285–293. [PubMed: 378407]

Petitprez F, de Reyniès A, Keung EZ, Chen TW, Sun CM, Calderaro J, Jeng YM, Hsiao LP, Lacroix L, Bougoüin A, et al. (2020). B cells are associated with survival and immunotherapy response in sarcoma. Nature 577, 556–560. [PubMed: 31942077]

Pulaski BA, and Ostrand-Rosenberg S (1998). Reduction of established spontaneous mammary carcinoma metastases following immunotherapy with major histocompatibility complex class II and B7.1 cell-based tumor vaccines. Cancer Res 58, 1486–1493. [PubMed: 9537252]

Qian J, Olbrecht S, Boeckx B, Vos H, Laoui D, Etlioglu E, Wauters E, Pomella V, Verbandt S, Busschaert P, et al. (2020). A pan-cancer blueprint of the heterogeneous tumor microenvironment revealed by single-cell profiling. Cell Res. 30, 745–762. [PubMed: 32561858]

Rodrigue-Gervais IG, Rigsby H, Jouan L, Sauvé D, Sékaly RP, Willems B, and Lamarre D (2010). Dendritic cell inhibition is connected to exhaustion of CD8+ T cell polyfunctionality during chronic hepatitis C virus infection. J. Immunol 184, 3134–3144. [PubMed: 20173023]

Ross R, Sudowe S, Beisner J, Ross XL, Ludwig-Portugall I, Steitz J, Tüting T, Knop J, and Reske-Kunz AB (2003). Transcriptional targeting of dendritic cells for gene therapy using the promoter of the cytoskeletal protein fascin. Gene Ther. 10, 1035–1040. [PubMed: 12776161]

Sautès-Fridman C, Petitprez F, Calderaro J, and Fridman WH (2019). Tertiary lymphoid structures in the era of cancer immunotherapy. Nat. Rev. Cancer 19, 307–325. [PubMed: 31092904]

Schoumacher M, El-Marjou F, Laé M, Kambou N, Louvard D, Robine S, and Vignjevic DM (2014). Conditional expression of fascin increases tumor progression in a mouse model of intestinal cancer. Eur. J. Cell Biol 93, 388–395. [PubMed: 25269996]

Shan D, Chen L, Njardarson JT, Gaul C, Ma X, Danishefsky SJ, and Huang XY (2005). Synthetic analogues of migrastatin that inhibit mammary tumor metastasis in mice. Proc. Natl. Acad. Sci. USA 102, 3772–3776. [PubMed: 15728385]

Sharma P, and Allison JP (2015). The future of immune checkpoint therapy. Science 348, 56–61. [PubMed: 25838373]

Sharonov GV, Serebrovskaya EO, Yuzhakova DV, Britanova OV, and Chudakov DM (2020). B cells, plasma cells and antibody repertoires in the tumour microenvironment. Nat. Rev. Immunol 20, 294–307. [PubMed: 31988391]

Smita S, Ahad A, Ghosh A, Biswas VK, Koga MM, Gupta B, Acha-Orbea H, and Raghav SK (2018). Importance of EMT Factor ZEB1 in cDC1 "MutuDC Line" Mediated Induction of Th1 Immune Response. Front. Immunol 9, 2604. [PubMed: 30483264]

Snyder M, Huang XY, and Zhang JJ (2011). Signal transducers and activators of transcription 3 (STAT3) directly regulates cytokine-induced fascin expression and is required for breast cancer cell migration. J. Biol. Chem 286, 38886–38893. [PubMed: 21937440]

Snyder M, Huang J, Huang XY, and Zhang JJ (2014). A signal transducer and activator of transcription 3$Nuclear Factor κB (Stat3$NFκB) complex is necessary for the expression of fascin in metastatic breast cancer cells in response to interleukin (IL)-6 and tumor necrosis factor (TNF)-α. J. Biol. Chem 289, 30082–30089. [PubMed: 25213863]

Steinman RM (1991). The dendritic cell system and its role in immunogenicity. Annu. Rev. Immunol 9, 271–296. [PubMed: 1910679]

Tan VY, Lewis SJ, Adams JC, and Martin RM (2013). Association of fascin-1 with mortality, disease progression and metastasis in carcinomas: a systematic review and meta-analysis. BMC Med 11, 52. [PubMed: 23442983]

Van Goethem E, Poincloux R, Gauffre F, Maridonneau-Parini I, and Le Cabec V (2010). Matrix architecture dictates three-dimensional migration modes of human macrophages: differential involvement of proteases and podosome-like structures. J. Immunol 184, 1049–1061. [PubMed: 20018633]

Wang Y, Zhang JJ, and Huang XY (2020). Anti-Metastasis Fascin Inhibitors Decrease the Growth of Specific Subtypes of Cancers. Cancers (Basel) 12, 2287.

Wei SC, Duffy CR, and Allison JP (2018). Fundamental Mechanisms of Immune Checkpoint Blockade Therapy. Cancer Discov 8, 1069–1086. [PubMed: 30115704]

West MA, Wallin RP, Matthews SP, Svensson HG, Zaru R, Ljunggren HG, Prescott AR, and Watts C (2004). Enhanced dendritic cell antigen capture via toll-like receptor-induced actin remodeling. Science 305, 1153–1157. [PubMed: 15326355]

Yamakita Y, Matsumura F, Lipscomb MW, Chou PC, Werlen G, Burkhardt JK, and Yamashiro S (2011). Fascin1 promotes cell migration of mature dendritic cells. J. Immunol 186, 2850–2859. [PubMed: 21263068]

Yamashiro S (2012). Functions of fascin in dendritic cells. Crit. Rev. Immunol 32, 11–21. [PubMed: 22428853]

Yamashiro-Matsumura S, and Matsumura F (1985). Purification and characterization of an F-actin-bundling 55-kilodalton protein from HeLa cells. J. Biol. Chem 260, 5087–5097. [PubMed: 3886649]

Yang S, Zhang JJ, and Huang XY (2009). Orai1 and STIM1 are critical for breast tumor cell migration and metastasis. Cancer Cell 15, 124–134. [PubMed: 19185847]

Yang S, Zhang JJ, and Huang XY (2012). Mouse models for tumor metastasis. Methods Mol. Biol 928, 221–228. [PubMed: 22956145]

Yang S, Huang FK, Huang J, Chen S, Jakoncic J, Leo-Macias A, Diaz-Avalos R, Chen L, Zhang JJ, and Huang XY (2013). Molecular mechanism of fascin function in filopodial formation. J. Biol. Chem 288, 274–284. [PubMed: 23184945]

Zhang Q, He Y, Luo N, Patel SJ, Han Y, Gao R, Modak M, Carotta S, Haslinger C, Kind D, et al. (2019). Landscape and Dynamics of Single Immune Cells in Hepatocellular Carcinoma. Cell 179, 829–845.e20. [PubMed: 31675496]

Zilionis R, Engblom C, Pfirschke C, Savova V, Zemmour D, Saatcioglu HD, Krishnan I, Maroni G, Meyerovitz CV, Kerwin CM, et al. (2019). Single-Cell Transcriptomics of Human and Mouse Lung Cancers Reveals Conserved Myeloid Populations across Individuals and Species. Immunity 50, 1317–1334.e10. [PubMed: 30979687]

Highlights

- Fascin inhibitors increase the number of intratumoral-activated dendritic cells

- Fascin inhibitors increase the antigen uptake by dendritic cells

- Fascin inhibitor treatment induces an inflamed tumor microenvironment

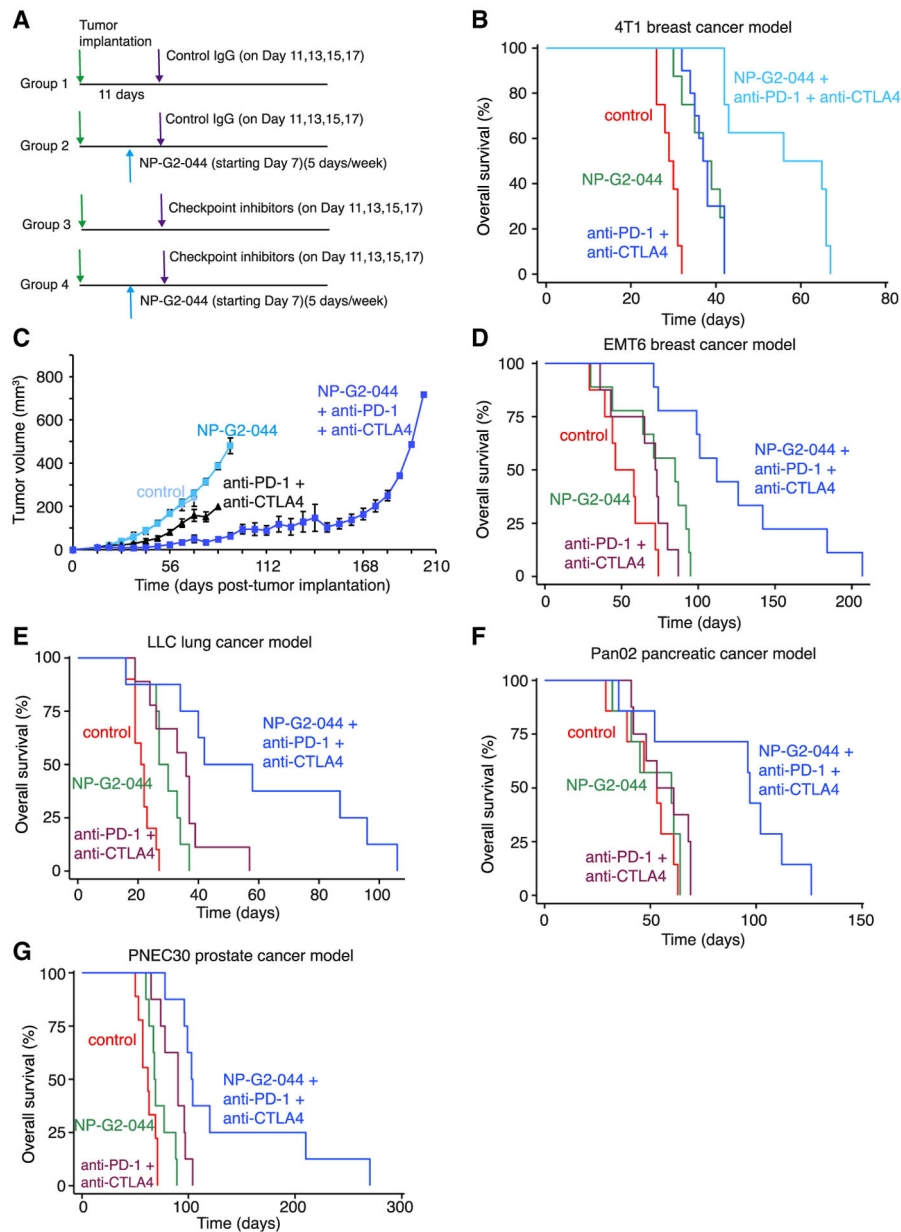- The inhibitor and anti-PD-1 antibody synergistically increase the overall survival

Figure 1. Fascin inhibitors together with immune checkpoint inhibitors synergistically increase the overall survival of tumor-bearing mice

(A and B) Combination treatments of fascin inhibitors with anti-PD-1 and anti-CTLA-4 antibodies synergistically increase the overall survival of mice bearing 4T1 mouse triple-negative breast tumor cells. (A) Scheme of treatments. (B) Overall survival data for the four groups of mice with different treatments (n = 8 or 10).

(C and D) Combination treatments of fascin inhibitors with anti-PD-1 and anti-CTLA-4 antibodies synergistically increase the overall survival of mice bearing EMT6 mouse triple-negative breast tumor cells. (C) Growth of primary tumors. Data are presented as mean ± SEM (n = 8 or 9). (D) Overall survival data for the four groups of mice with different treatments (n = 8 or 9).

(E) Combination treatments of fascin inhibitors with anti-PD-1 and anti-CTLA-4 antibodies synergistically increase the overall survival of mice bearing LLC mouse lung cancer cells (n = 8–10).

(F) Fascin inhibitors with anti-PD-1 and anti-CTLA-4 antibodies synergistically increase the overall survival of mice bearing Pan02 mouse pancreatic cancer cells (n = 7 or 8).

(G) NP-G2–044 with anti-PD-1 and anti-CTLA-4 antibodies increase the overall survival of mice bearing PNEC30 mouse prostate cancer cells (n = 8 or 9).
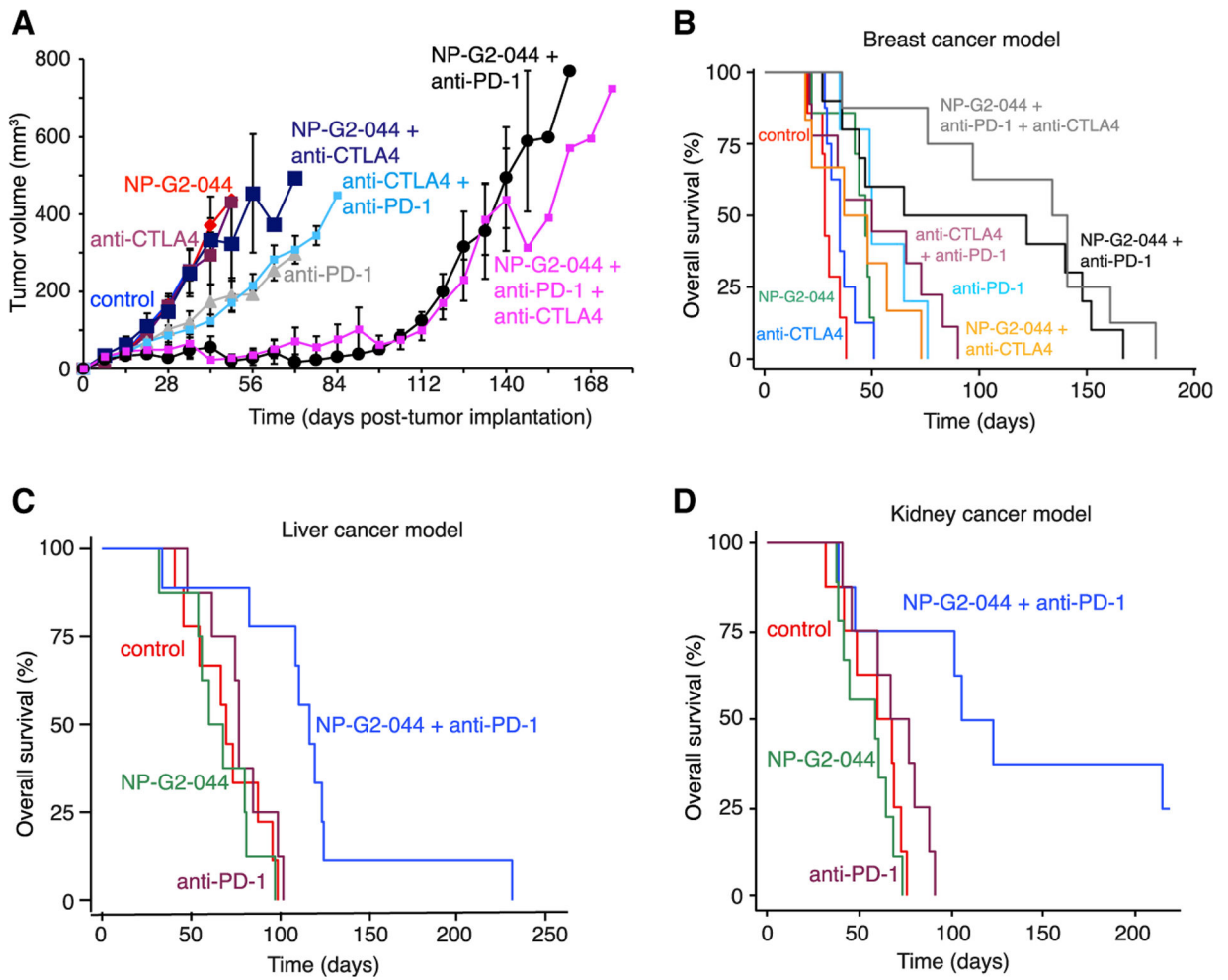
Figure 2. NP-G2–044 and anti-PD-1 antibody synergistically increase the overall survival of tumor-bearing mice

(A and B) The synergistic effect is due to the combination of fascin inhibitors and anti-PD-1 antibody. (A) 4T1 primary tumor growth from the eight groups of mice with different treatments. All mice were monitored till death. Data are presented as mean ± SEM (n = 6–10). (B) Overall survival of the eight groups of mice with different treatments (n = 6–10).

(C) Overall survival data of mouse models of Hepa1–6 liver cancer (n = 8 or 9).

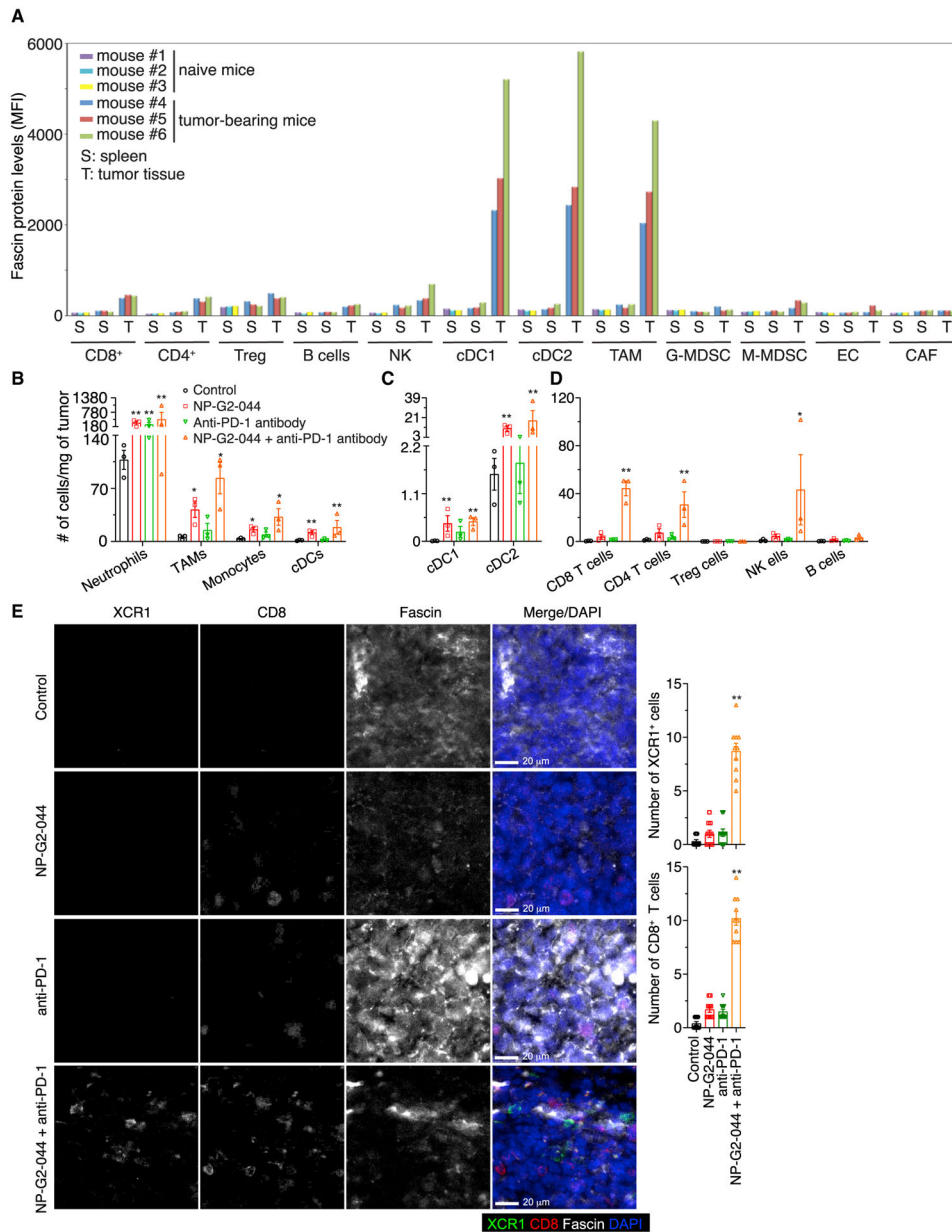(D) Overall survival data of mouse models of Renca kidney cancer (n = 8 or 9).

Figure 3. Accumulation of intratumoral DCs after NP-G2–044 treatment

(A) Elevated expression of fascin protein in intratumoral DCs. Expression of fascin protein in different types of cells from the spleen (S) of naive mice (the first three columns), the S of the 4T1 tumor-bearing mice (the middle three columns), and the tumor tissues (T) of the tumor-bearing mice (the last three columns). Tumor tissues were dissected on day 20.

(B–D) Immune cell composition within the tumor microenvironment. Tumor tissues from four groups of 4T1 tumor-bearing mice (control, NP-G2–044 treated, anti-PD-1 antibody treated, and treatment with NP-G2–044 + anti-PD-1 antibody) were analyzed by FACS for different types of immune cells. Tumor tissues were dissected on day 25.

(E) Immunofluorescence imaging analysis of the tumor tissues from four groups of 4T1 tumor-bearing mice (control, NP-G2–044 treated, anti-PD-1 antibody treated, and treatment

with NP-G2–044 + anti-PD-1 antibody). Anti-XCR1 antibody (for cDC1 cells), anti-CD8 antibody (for CD8$^+$ T cells), anti-fascin antibody (for tumor cells), and DAPI were used. Right: quantification of XCR1$^+$ or CD8$^+$ cells per imaging field (data presented as mean ± SEM; each with 10 fields). Tumor tissues were dissected on day 25. n = 3 mice. Scale bars, 20 μm. *p < 0.05; **p < 0.005. One-way analysis of variance (ANOVA) followed by the Dunnett's test, compared with the control group.
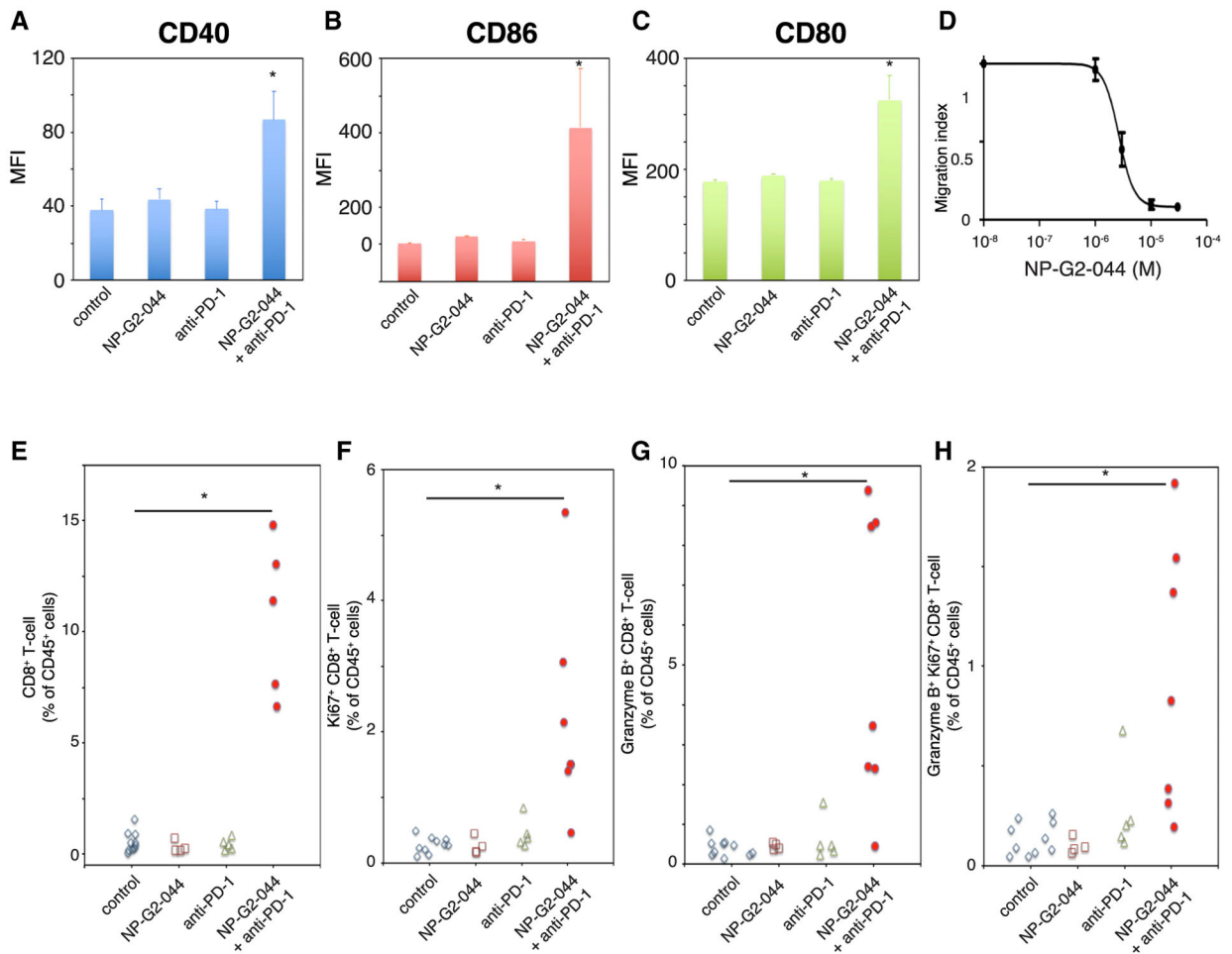
Figure 4. Increases of intratumoral activated DCs and CD8$^+$ T cells

(A–C) Numbers of DCs with activation markers CD40 (A), CD86 (B), or CD80 (C). These DCs were from spleen or 4T1 tumor tissues isolated from mice treated with fascin inhibitors and anti-PD-1 antibody or from control mice. Data are presented as mean ± SEM (n = 3). *p < 0.05 (Student's t test).

(D) Inhibition of DC migration by fascin inhibitors. Data are presented as mean ± SEM (n = 3).

(E–H) Increase of intratumoral CD8$^+$ T cells by the combination treatment of NP-G2–044 + anti-PD-1 antibody. Increases of the numbers of total CD8$^+$ T cells (E), proliferating Ki67$^+$ CD8$^+$ T cells (F), activated Granzyme B$^+$ CD8$^+$ T cells (G), as well as proliferating and activated (Ki67$^+$Granzyme B$^+$) CD8$^+$ T cells (H) are shown from 4T1 tumor tissues. Each filled circle represents one mouse. Tumor tissues were dissected on day 27. *p < 0.05 (Student's t test).
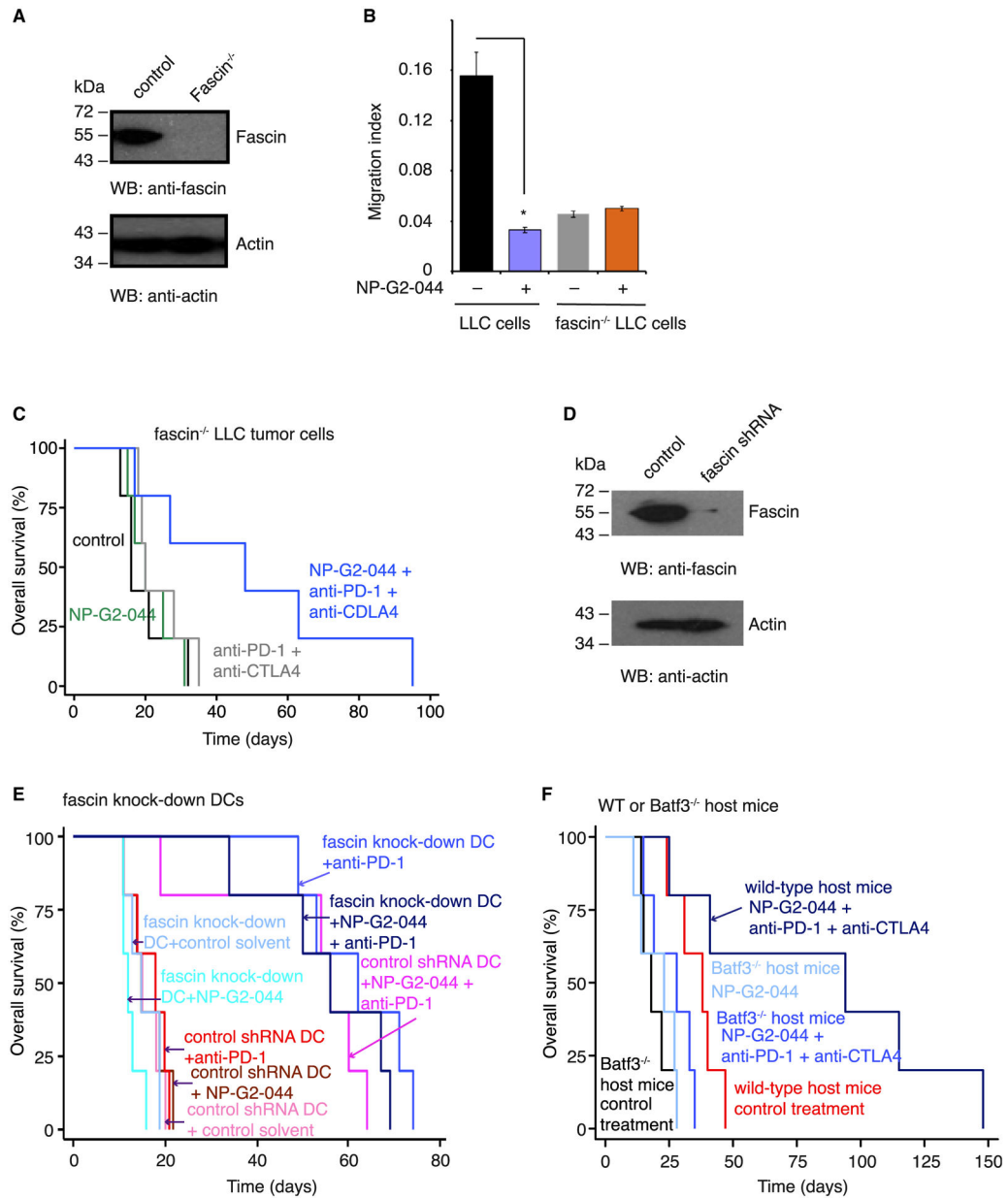
Figure 5. Fascin in DCs, but not in tumor cells, is essential for the synergistic immune response

(A) Western blots show that fascin protein is absent in fascin gene knockout (by CRISPR) LLC cells.

(B) Although NP-G2044 blocked the migration of wild-type LLC cells, it had no effect on the migration of LLC cells with fascin gene knockout. Data are presented as mean ± SEM (n = 3). *p < 0.05 (Student's t test).

(C) Overall survival data of four different groups of mice after administering *fascin*^{−/−} LLC tumor cells into the lungs (n = 5).

(D) Western blot shows fascin protein levels were reduced in fascin shRNA-treated DC cells compared with control shRNAs-treated DCs.

(E) Overall survival of mice with DCs that expressed fascin shRNAs or control shRNAs. After LLC tumor cell implantation, the mice were treated with control solvent, NP-G2–044, anti-PD-1 antibody, or with the combination therapy of NP-G2–044 + anti-PD-1 antibody (n = 5).

(F) Overall survival study of *Batf3*$^{-/-}$ mice treated with NP-G2–044 or NP-G2–044 + ICIs after LLC tumor cell implantation. As a control, wild-type mice were implanted with LLC tumor cells and treated with control IgG or with NP-G2–044 + ICIs (n = 5).
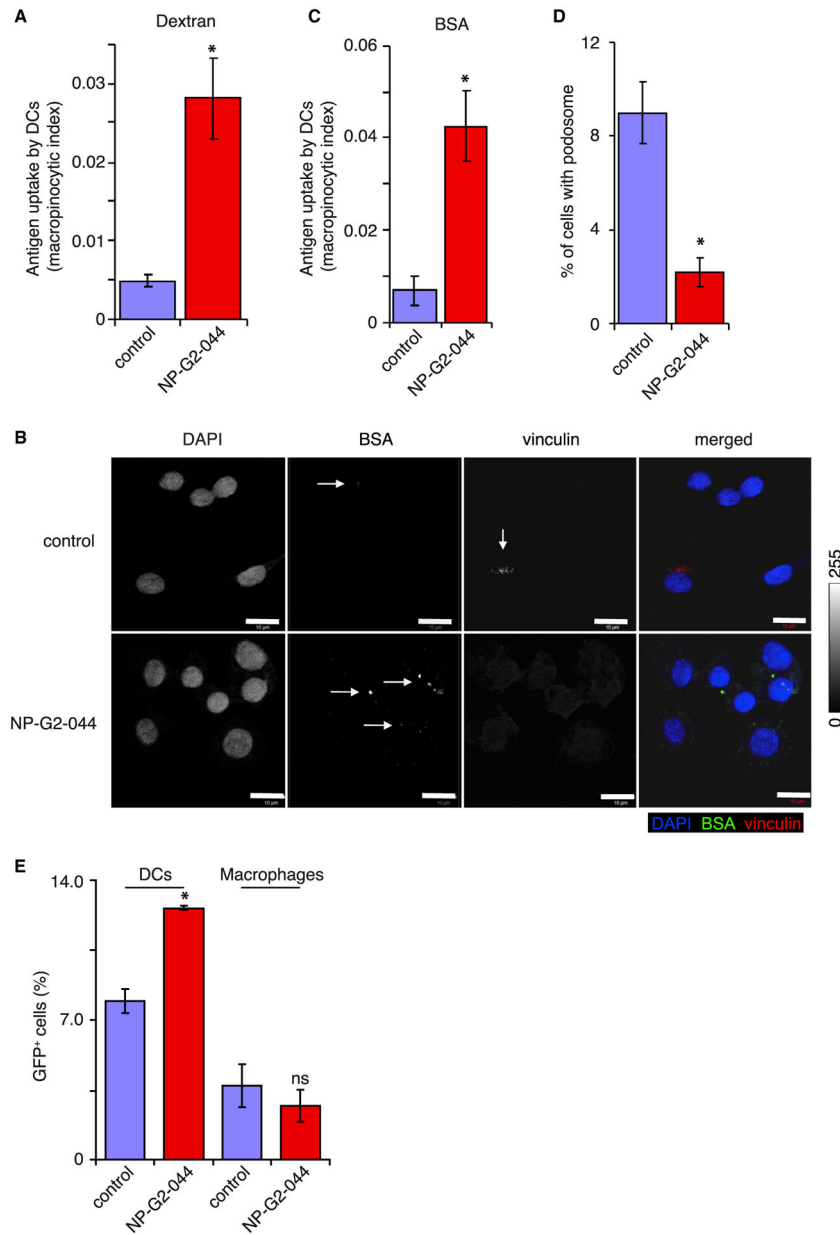
Figure 6. NP-G2–044 increases the antigen uptake by DCs

(A–D) NP-G2–044 increased the antigen uptake by DCs. Fluorescently labeled dextran (A) or BSA (B and C) was added to cultured cDC1 cells. The uptake of dextran or BSA was quantified. In (A), 106 cells in the control group and 68 cells in NP-G2–044-treated group were quantified. In (C), 88 cells from the control group and 32 cells from NP-G2–044-treated group were quantified. *p < 0.05 (Student's t test). (B and D) NP-G2–044 inhibited podosome formation in DCs. (B) Immunofluorescent staining of podosomes by anti-vinculin antibody was colored red. Fluorescently labeled BSA (green) was added to cultured cDC1 cells. Fluorescently labeled BSA was marked by arrows. Scale bars, 10 μm. (D) A total of 728 cells in the control group and 713 cells in NP-G2–044-treated group were quantified. The percentage of cells with podosomes is shown. *p < 0.05 (Student's t test).

(E) GFP-labeled 4T1 mouse breast tumor cells were implanted into the mammary fat pad. GFP$^+$ DCs or macrophages within tumor tissues were quantified. *p < 0.05 (Student's t test). ns, not significant. n = 3. Data are shown as mean ± SEM.
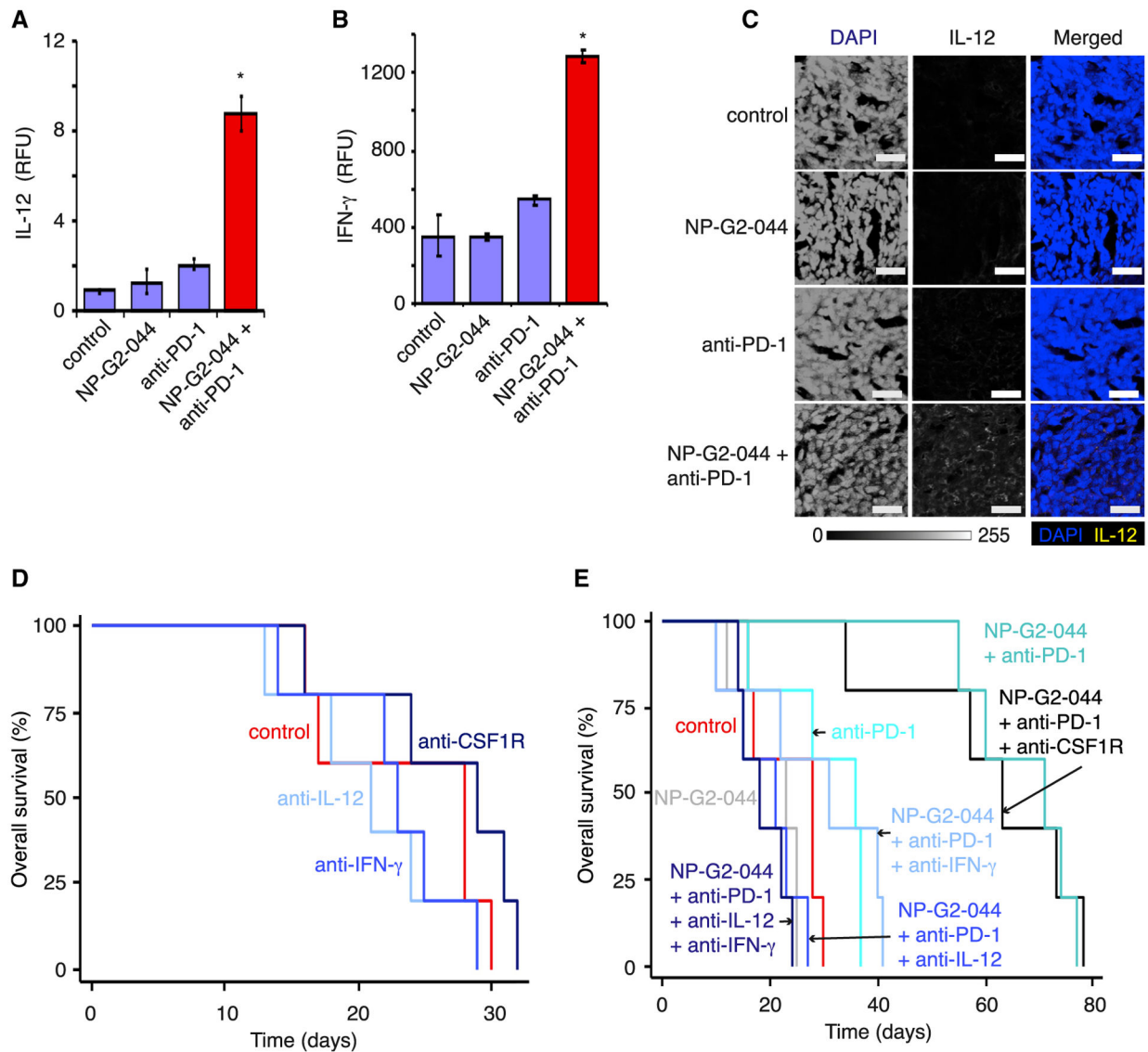
Figure 7. IL-12 and IFN-γ are necessary for the synergistic anti-tumor effect of NP-G2–044 + anti-PD-1 antibody

(A and B) Relative fluorescence units (RFUs) of IL-12 (A) and INF-γ (B) were quantified in tumor tissues from the four groups of mice. Data are presented as mean ± SEM. *p < 0.05 (110 regions of interest [ROIs]) (Student's t test).

(C) Immunofluorescence imaging analysis of the tumor tissues from four groups of LLC tumor-bearing mice (control, NP-G2–044 treated, anti-PD-1 antibody treated, and treatment with NP-G2–044 + anti-PD-1 antibody). Anti-IL-12 antibody and DAPI were used. Tumor tissues were dissected on day 23. Scale bars, 20 μm.

(D and E) Neutralizing IL-12 and IFN-γ, but not CSF1R, abolished the anti-tumor effect of NP-G2–044 + anti-PD-1 antibody. Data shown in (D) and (E) are from the same experiment. The data from some groups are shown in (D) to avoid the overcrowding in (E). The data for the control group in (D) and (E) are the same. The only two groups that show statistical significance (log-rank test, p < 0.05) from the control group are the NP-G2–044 + anti-PD-1

treatment group and the NP-G2–044 + anti-PD-1 + anti-CSF1R treatment group. Five mice per group.

KEY RESOURCES TABLE

REAGENT or RESOURCE	SOURCE	IDENTIFIER
Antibodies		
Anti-Vinculin	Santa Cruz Biotechnology	Cat#sc-7648
Anti-Fascin 1 (D-10)	Santa Cruz Biotechnology	Cat#sc-46675
Anti-XCR1	Biolegend	Cat#148210
Anti-Fascin 1 (D-10) PE	Santa Cruz Biotechnology	Cat#sc-46675 PE
Anti-CD172a	Biolegend	Cat#144014
Anti-mouse PD-1	Bio X Cell	Cat#BE0146
Anti-mouse CSF1R	Bio X Cell	Cat#BE0213
Anti-mouse IFNγ	Bio X Cell	Cat#BE0055
Anti-mouse IL-12 p40	Bio X Cell	Cat#BE0051
Anti-mouse CTLA-4	Bio X Cell	Cat#BE0131
rat IgG2a Isotype Control	Bio X Cell	Cat#BE0089
Polyclonal Syrian hamster IgG	Bio X Cell	Cat#BE0087
CD45 Monoclonal Antibody (30-F11)	eBioscience	Cat#64-0451-82
CD170 (Siglec F) Monoclonal Antibody	eBioscience	Cat#50-1702-82
Anti-CD4	Biolegend	Cat#100532
Anti-B220(CD45R) - PE	eBioscience	Cat#12-0452-82
Anti-CD4	eBioscience	Cat#78-0048-12
Anti-CD25	eBioscience	Cat#45-0251-82
Anti-CD31	eBioscience	Cat#25-0311-81
Anti-CD140a	eBioscience	Cat#17-1401-81
Anti-Foxp3	eBioscience	Cat#48-5773-80
Anti-Ki67	eBioscience	Cat#41-5698-80
Anti-NKp46	eBioscience	Cat#11-3351-82
Anti- PD-L1	eBioscience	Cat#25-5982-82
Anti-B220	Biolegend	Cat#13-0452-82
Anti-CD11b	Biolegend	Cat#67-0112-82
Anti-CD11c	Biolegend	Cat#48-0114-82
Anti-CD8	Biolegend	Cat#100741
Anti-CD40	Biolegend	Cat#102912
Anti-CD80	Biolegend	Cat#104810
Anti-CD86	Biolegend	Cat#105012
Anti-Ly6C	Biolegend	Cat#128026
Anti-Ly6G	Biolegend	Cat#217618
Anti-MHC II	Biolegend	Cat#107639
Anti-PD-1	Biolegend	Cat#109109
Anti-TCRb	Biolegend	Cat#109241
Anti-Granzyme B	invitrogen	Cat#GBR05
Anti-CD8a	Biolegend	Cat#10078
Anti-Fascin 1 (D-10) AF647	Santa Cruz Biotechnology	Cat#sc-46675AF647

REAGENT or RESOURCE	SOURCE	IDENTIFIER
Goat Anti-Rat IgG H&L (Alexa Fluor® 568)	abcam	Cat#ab175476
Anti-CD21	BD Biosciences	Cat#561770
Rhodamine (TRITC) AffiniPure Donkey Anti-Goat IgG (H+L)	Jackson ImmunoResearch Inc	Cat#705-025-147
Anti-F4/80	BD Biosciences	Cat#565613
Chemicals, peptides, and recombinant proteins		
Alexa Fluor 488 phalloidin	invitrogen	Cat#A12379
rm GM-CSF	R&D systems	Cat#415-ML
rm IL-4	R&D systems	Cat#404-ML
CD11c MicroBeads Ultrapure Mouse	Miltenyi Biotec	Cat#130-108-338
MISSION® pLKO.1-puro Empty Vector Control Plasmid DNA	Sigma-Aldrich	Cat#SHC001
FSCN1 MISSION shRNA Plasmid DNA	Sigma-Aldrich	Cat#TRCN0000335363
Cascade Blue™ Dextran	Thermo Fisher	Cat#D7132
Alexa Fluor 488 BSA	Thermo Fisher	Cat#A13100
Bovine Type I Atelo-Collagen Solution	Advanced BioMatrix	Cat#5133–20ML
Permeable Support for 24 Well Plate with 8.0 μm Transparent PET Membrane	Falcon	Cat#353097
Oligonucleotides		
LentiCRISPRv2-fascin (KO#2)-guide: CACAGCCTCTGCCGTGCCGT	This paper	N/A
Experimental models: organisms/strains		
Mouse: BALB/c	Charles River Labs	Strain Code 028
Mouse: C57BL/6	Jackson Lab	Stock No: 000664
Mouse: *Batf3*–/–	Jackson Lab	Stock No: 013755
Experimental models: cell lines		
Mouse: cell line 4T1	ATCC	CRL-2539
Mouse: cell line LLC	ATCC	CRL-1642
Mouse: cell line PNEC30	ATCC	CRL-2930
Mouse: cell line EMT6	McDonald et al., 2017	N/A
Mouse: cell line Pan02	Costa-Silva et al., 2015	N/A
Mouse: cell line Hepa1–6	Ersoy et al., 2018	N/A
Mouse: cell line Renca	Martis et al., 2018	N/A
Mouse: cell line cDC1	Fuertes Marraco et al., 2012	N/A